Development and Verification of an Anthropomorphic Mechanical Finger Model in OpenSim

Incorporating Joint-Ligament System, and Interphalangeal Joint Coupling Mechanism

Rana Sabina Ul Haq

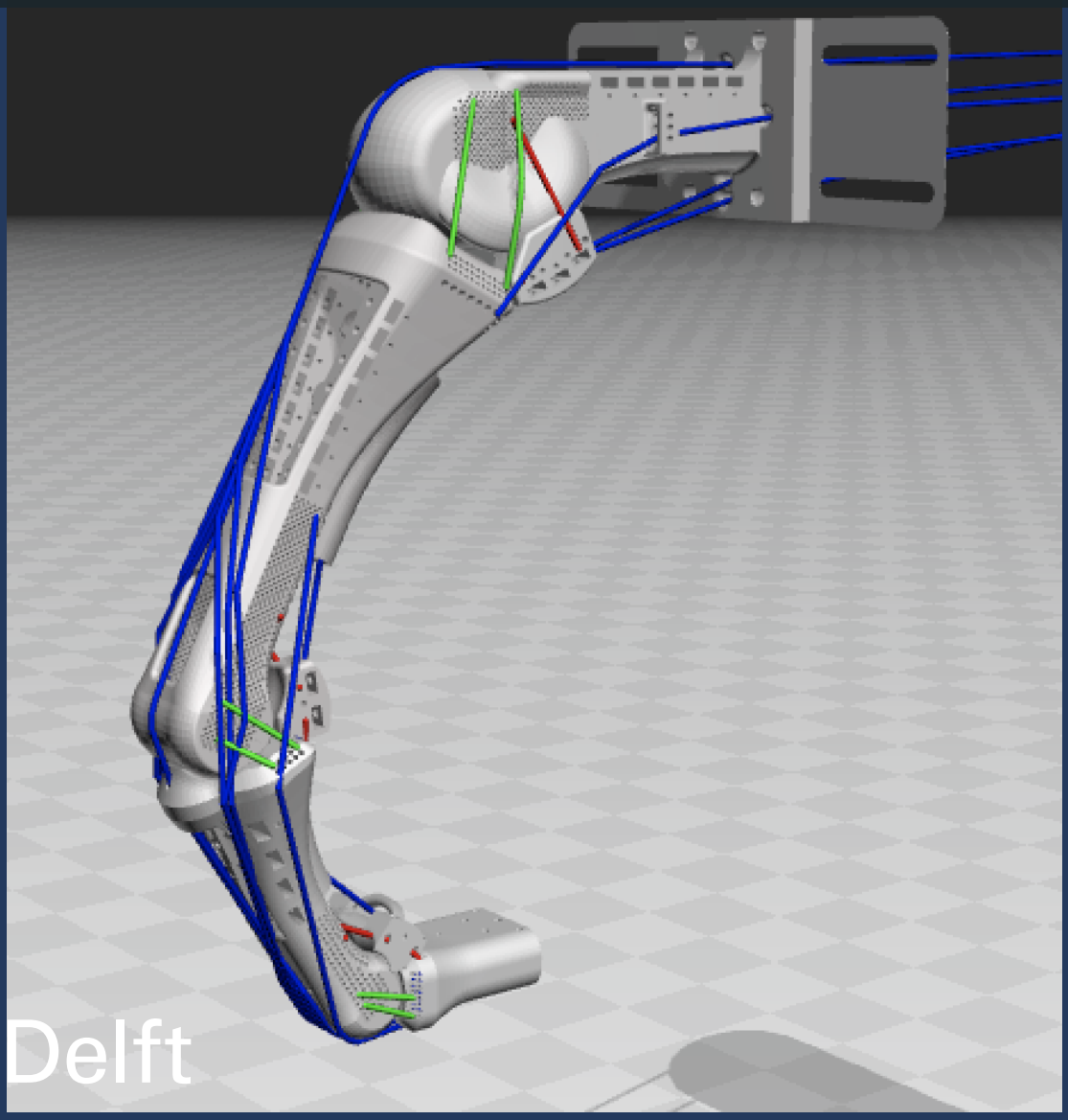

TU Delft

Development and Verification of an Anthropomorphic Mechanical Finger Model in OpenSim

Incorporating Joint-Ligament System, and Interphalangeal Joint Coupling Mechanism

Thesis report

by

Rana Sabina Ul Haq

to obtain the degree of Master of Science
at the Delft University of Technology
to be defended publicly on September 25th, 2024 at 09:00 AM

Supervisors:	Dr. Ir. G. Smit (TU Delft)
	Dr. Ir. A. Seth (TU Delft)
External member:	Dr. Ir. F.J.H.Gijsen (TU Delft)
Place:	Faculty of Mechanical Engineering, Delft
Student number:	4699122

An electronic version of this thesis is available at `http://repository.tudelft.nl/`.

Faculty of Mechanical Engineering · Delft University of Technology

Summary

Background Computational musculoskeletal models are valuable for understanding finger biomechanics and aiding in medical applications such as postoperative therapy and surgical planning. These models simulate various scenarios and predict outcomes by representing the biomechanical system through equations of motion. However, the complex mechanics of the human finger, particularly the role of the Lateral Bands in coordinated joint flexion, have primarily been studied in static simulations. Their role in dynamic simulations, especially with the inclusion of other key tendons and ligaments, has not been researched.
Aim This study aims to develop a musculoskeletal model to enhance our understanding of the contribution of Lateral Bands to coordinated finger flexion, by combining insights from previous research to address existing gaps in finger biomechanics. The model will replicate the anatomical joints and Lateral Band structures of an anthropomorphic mechanical finger, offering a simplified design to reduce simulation complexity and enhance verification reliability.
Method An adapted anthropomorphic mechanical finger was created based on previous work, scaled down to reduce weight and required actuation force. The simulation model was developed in OpenSim, using bone geometries from CAD files and direct measurement attachment location of tendons and ligaments from the mechanical finger for improved accuracy. Model verification involved comparing the model's behavior with the mechanical finger through experiments focusing on finger flexion under external deep flexor tendon load, using motion capture data, inverse kinematics (IK), and forward dynamics (FD).
Results The simulation model accurately replicated the mechanical finger's joint kinematics, with an average squared error ranging from 1.54e−3 mm to 9.55e−3 mm and an average marker RMSE of $\pm$0.65 mm. Tendon displacement and moment arm were verified with average errors $\pm$1 mm and $\pm$1.23 mm, respectively, indicating that the model closely matches the mechanical finger's tendon force and joint torque relationships. The model demonstrated that Lateral Bands are essential for interphalangeal joint (IPJ) coupling, as they adjust their tension by becoming taut or slack during finger flexion to distribute forces effectively. Without these Lateral Bands, finger flexion leads to unrealistic joint movements in mechanical finger models. Additionally, the Lateral Bands play a significant role in generating tension in the deep flexor tendon during IPJ coupling.
Conclusion This study demonstrated the role of Lateral Bands during dynamic finger flexion by incorporating anatomically-based structures and replicating their behavior. The findings provide deeper insights into their function and set a new foundation for future research. Additional studies could further explore how Lateral Bands influence force distribution and joint mechanics, potentially leading to better understanding and treatment of finger injuries and disorders.

Contents

Nomenclature

List of Abbreviations

2D	Two-dimensional
3D	Three-dimensional
CS	Central slip (similar to proximal slip)
CT	Computed tomography (scans)
DIP	Distal interphalangeal
DoF	Degrees of freedom
EA	Extensor apparatus
ED	Extensor digitorum communis
EI(P)	Extensor indicis (propius)
EMG	Electromyographic
FD	Forward Dynamics
FDP	Flexor digitorum profundus
FDS	Flexor digitorum superficialis
IK	Inverse Kinematics
IP	Interphalangeal
IPJ	Interphalangeal joint
LUM	Lumbrical
MAE	Mean absolute error
MAJE	Mean absolute joint error
MCP	Metacarpophalangeal
ORL	Oblique retinacular ligament
PIP	Proximal interphalangeal
RB	Radial lateral band
RIO	Radial interosseous (similar to Dorsal interosseous (DI))
SD	Standard deviation
TE	Terminal extensor
UB	Ulnar lateral band
UIO	Ulnar interosseous (similar to Palmar interosseous (PI))

List of Figures

List of Tables

1

Introduction

1.1. Musculoskeletal Modelling

Fingers play an important role in a wide range of activities, from fine motor tasks like writing and playing musical instruments to high-stress activities such as rock climbing and heavy lifting [1]. The anatomy of the fingers that enable this wide range of function (Figure 2.2) is explained in Chapter 2. When injuries or deformities occur, effective surgical intervention depends on a deep understanding of the finger biomechanics. For example, finger deformities such as swan neck, boutonniere, and mallet finger often resulted from ruptures in connective tissues can lead to imbalances in force distribution, impairing finger movement and overall function [2]. This highlights that force distribution, one of many aspects of human finger biomechanics, is important to understand and is usually difficult to obtain from experiments on human fingers [3].

Computational musculoskeletal models have the potential to provide better insights and understanding of the biomechanics of the finger, with the potential to aid medical applications, such as postoperative therapy and surgical planning for joint deformities [4, 5]. These models are computational representations of the biomechanical system, consisting of bones, muscles, and joints, described as a set of equations of motion. When solving these equations, the model kinematics and dynamics can be solved depending on the model state or when an external input is applied. For example, experimental motion data can be given as input to the simulation model to determine muscle forces for a desired movement. Musculoskeletal models are tools that can provide insight on the biomechanics (motor control) and anatomy of the human body, making it a subject of extensive research and study. For example, these models enable researchers to simulate various scenarios and predict joint movement or overall performance when one or more components change, such as how joint motion is affected by tendon removal or injury, making them highly useful for clinical applications. However, to use these models, they must first undergo extensive verification and validation to ensure they are reliable for identifying the functions of specific structures and suitable for clinical use.

While musculoskeletal models have advanced in many areas, the human finger is still unsurpassed in its complexity, particularly due to its complex tendon network, joint kinematics, and their underlying mechanism of the interdependency of joints. Current models are often limited in capturing the detailed mechanics of specific structures, such as the Lateral Bands, which play a critical role in coordinated finger flexion. This creates a need for improved musculoskeletal models that can better represent these interactions. Therefore, this research aims to explore how computational musculoskeletal models can be enhanced to further our understanding of the function and interactions of Lateral Bands in producing coordinated finger movement, providing deeper insights into finger biomechanics that are essential for both clinical applications and biomechanical studies.

1.2. Existing Musculoskeletal Skeletal Models

1.2.1. Joint Kinematics

Over the past decade, several musculoskeletal models have been developed based on cadaveric studies to create finger models. Typically, finger bones are represented as a series of rigid bodies or segments connected by joints (Figure 1.1). These joints are often modelled as idealized mechanical joints, such as hinges or universal joints, which allow movement in one or two planes, specifically flexion-extension and

abduction-adduction, constraining it to the physiological joint rotation. Many models also include passive joint properties, to account for the passive resistance of intrinsic soft tissues, such as ligaments, skin, intrinsic muscles, and joint capsules. However, these are modelled into a single torque value that varies with joint position [6, 7, 8], and do not isolate the contributions of individual parts. In reality, human fingers have anatomical joints which more complex than simple hinge joints because they do not rotate around a fixed pin. Instead, they have cartilaginous surfaces that slide over each other during finger movement and are mechanically stabilized by connective tissues, such as joint ligaments, which help constrain the joint's range of motion.

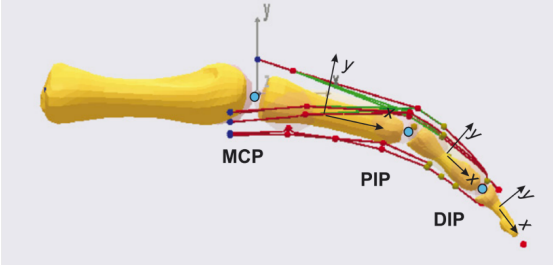

Figure 1.1: Musculoskeletal model of the finger developed in software AnyBody, three joints (MCP, PIP and DIP) and includes seven muscles-tendons [9].

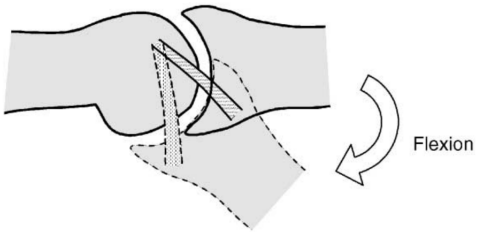

Figure 1.2: Flexion at the MCP joint, the collateral ligament becomes taut during flexion [10].

An inverse dynamics model developed by Sancho-Bru et al. (2001) incorporates the collateral ligaments separately into the model [10, 11] accounting for the coupled effects of flexion-extension and abduction-adduction in the MCP joint. During flexion, these ligaments become taut (Figure 1.2), reducing the range of lateral movement. During abduction-adduction, tension increases in these ligaments, generating an additional moment at the MCP joint [10]. In this model, the ligaments are represented as straight lines that connect the metacarpal to the proximal phalanx.

1.2.2. Implementation of the Extensor Mechanism

The tendons in the fingers form a complex and intricate network known as the extensor mechanism (EM), responsible for transmitting and distributing forces to the finger bones generated by the muscles. This network interconnects the intrinsic and extrinsic muscles by linking the distal tendons of palmar interosseous, lumbrical, and extensor digitorum muscles[12] (Figure 2.2). Determining the internal force distribution in the EM directly from in vitro measurements presents challenges due to potential damage to fibres and the difficulty in measuring fibre slack or tautness during flexion with the available measuring resolution [13, 3]. Consequently, studies have mainly focused on determining this tendon force distribution in the EM during static simulation, often using optimization methods, for various finger poses. Many models implement the extensor mechanism based on Winslow's rhombus tendon network (Figure 1.3) which is a simplified representation of this intricate network [14, 5, 15, 12, 16, 17, 3, 18, 19]. An example, shown in Figure 1.4, shows a novel adaptation of Winslow's rhombus tendon network modelled in OpenSim [15]. This model uses a static optimization approach to estimate the force distribution within the tendon network, aiming to minimize the discrepancy between experimental and predicted data. However, a recent OpenSim model of the hand and wrist, including the finger, has not adopted this approach. This model omits the

extensor mechanism (EM) due to limitations in modeling the intersecting bands of the EM, resulting in the use of separate paths sharing the same trajectory [15]. Including the EM with this approach would increase the number of muscle-tendon actuators and require additional constraints for force distribution [6].

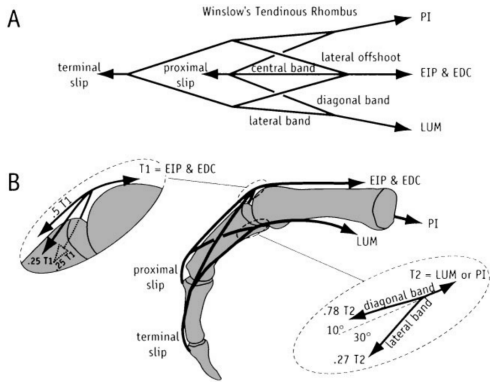

Figure 1.3: Winslow's Rhombus Tendon Network [19], a simplified representation of the Extensor Mechanism (EM) (Figure 2.2). This illustrates how the interactions between flexor and extensor tendons merge into distinct bands—central, terminal, and Lateral Bands. These bands converge and are arranged geometrically throughout the finger, distributing tendon forces effectively across the finger.

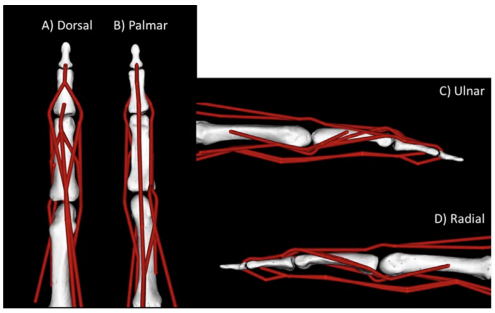

Figure 1.4: Extensor mechanism, modeled in OpenSim [15], uses multiple separate paths sharing the same muscle-tendon trajectory

Lastly, an important part of finger mechanics is the interphalangeal joint (IPJ) coupling, which refers to the interdependence between PIP and DIP joints during finger flexion. Leijnse and Spoor (2012) incorporated this coupling mechanism by developing a 2D kinematic finger model with individual strings that focusses on the lateralbands of extensor mechanism (EM), and discusses its relation to the IPJ coupling mechanism (Figure 1.5 and Figure 2.5 from Chapter 2). The IPJ coupling is modeled as a mathematical constraint, with the coupling dependent on factors such as moment arms, relative lengths, and the curvature of the phalanges. The attachment locations and lengths of the model strings (e.g., Lateral Bands) are varied by fitting the model to experimental data [13]. Moreover, an EM model developed by Dogadov et al. (2022), consisting of Lateral Bands, demonstrated that the forces in the Lateral Bands vary according to finger posture in a static simulation [20].

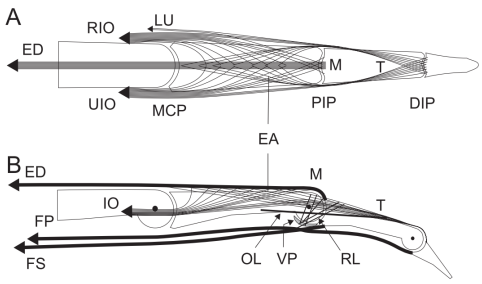

Figure 1.5: Finger extensor mechanism, Leijnse and Spoor (2012) model consist of T (tendon strings), OL (oblique retinacular ligament), RL (retinacular ligament) [13].

1.3. Anthropomorphic Robot Fingers

While simulation models based on cadaveric studies offer a close approximation of reality, they face limitations such as limited availability and consistency of anatomical data. These issues arise from cadavers anatomical variability, degradation over time, and inconsistencies in data due to factors like skin and tissue conditions, leading to uncertainties in model parameters and validation [21, 22]. An emerging alternative involves anthropomorphic robotic fingers, which are becoming increasingly anatomically accurate [23, 24, 21, 25, 26, 27]. These robotic models offer a valuable means of validation, as they avoid many of the limitations associated with cadaver studies and provide consistent data for verification of the accuracy and effectiveness of musculoskeletal simulations. To the author's best knowledge, there are currently only a limited number of musculoskeletal models evaluated against robotic fingers. However, these models often use robotic fingers with pin joints rather than anatomical joints, which limits their ability to accurately reflect the complex biomechanics of the human finger. For example, Niehues et al. modelled interconnected tendon networks, using a spring framework for both forward and inverse simulations. Their approach applies optimization to address the interconnection within the EM tendons, using an iterative method to manage the indeterminate and pose-dependent force distribution [25]. Another model, developed by Tigue et al. (2019), used bond-graph modelling for quasi-static finger simulations [28]. However, neither of these models conducts dynamic simulations that fully integrate all the structures of the human finger, including anatomical joints and with the IPJ coupling mechanism.

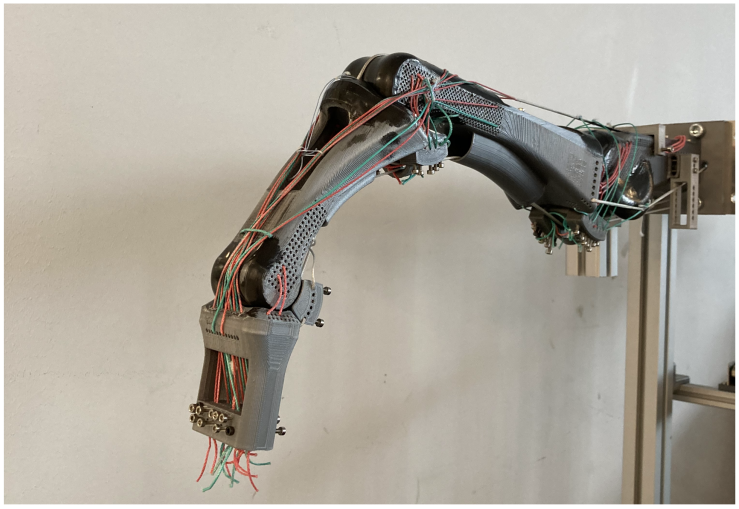

Figure 1.6: Anthropomorphic robot finger developed by van Ooijen (2022) [24]. This finger contains the primary tendons responsible for flexion and extension. Its humanoid joint-ligament system is designed to rotate around the curvature of the joint. The ligaments provide joint stability and constrain the range of motion by tightening or loosening based on the joint angle. Additionally, lateral bands, which are separate strings originating from the main extensor tendon, are incorporated. These bands adjust their tension to facilitate the interphalangeal joint coupling, as observed in human fingers.

In a previous project at TU Delft, a fully manipulable anthropomorphic robot finger was developed to replicate the functional and anatomical characteristics of a human finger [24]. The design was simplified to resemble a real human finger, focusing on the main tendons without incorporating the lumbrical muscles. The extensor mechanism was formed by Lateral Bands originating from the extensor tendon, contributing to IPJ coupling. CT scans of a dissected finger were used to create detailed 3D models in SolidWorks, defining joint geometries and soft tissue attachment points. The design featured anatomical joints with a (semi)spherical head and socket for articulation, along with perforations for ligament attachments to ensure proper joint range of motion. The final assembly demonstrated proper joint movement and IPJ coupling (Figure 1.6). Thus, this project provided the basis of the development and verification of the musculoskeletal model of this study.

1.4. Problem Statement

Previously described musculoskeletal models, as summarised in the previous section, incorporate joints by not explicitly representing the physical ligaments, the extensor mechanism (EM) with optimization methods and the interphalangeal joints (IPJs) coupling with mathematical constraints during static simulations. As a result, these models provide valuable insights into individual components, but limit their ability to accurately reflect the complex biomechanics of the human finger. Recent development of an anthropomorphic (robot) finger included these anatomical joints with a humanoid joint-ligament system and incorporated individual strings to recreate the IPJ coupling mechanism.
This presents a research opportunity to develop and verify a musculoskeletal model based on this anthropomorphic finger, using the OpenSim environment, which is a widely-used platform to perform such dynamic simulation, like Forward Dynamics. Thus, combining the ideas of previous researches to create a model that can potentially address the aforementioned gaps and provide further insights into the biomechanics of the human finger.

1.5. Research Aim

How can computational musculoskeletal models be improved to further understand the function of Lateral Bands and their interactions in producing coordinate finger flexion?

To answer this question, this study aims to develop a musculoskeletal model in OpenSim that replicates the anatomical joints and Lateral Band structures represented by an anthropomorphic mechanical finger. This mechanical finger is beneficial because it incorporates simplifications that reduce the complexity of developing the simulation model, enhance the reliability of the model, and enable its verification. To ensure that, its performance will be verified by comparing its dynamic simulations of finger joint flexion with experimental data from the mechanical finger.

1.6. Report Outline

The structure of this study is outlined in Figure 1.7. Chapter 2 covers the anatomy and their function of the human finger, forming the basis for the mechanisms behind the anthropomorphic mechanical finger and the OpenSim model. Chapter 3 details the construction of the mechanical finger, while Chapter 4 focuses on the development of the musculoskeletal finger model in OpenSim. Chapter 5 explains the methodology and experiments conducted for verification. The results are presented in Chapter 6, followed by a disccusion in Chapter 7, along with recommendations. Finally, Chapter 8 provides the study's conclusion.

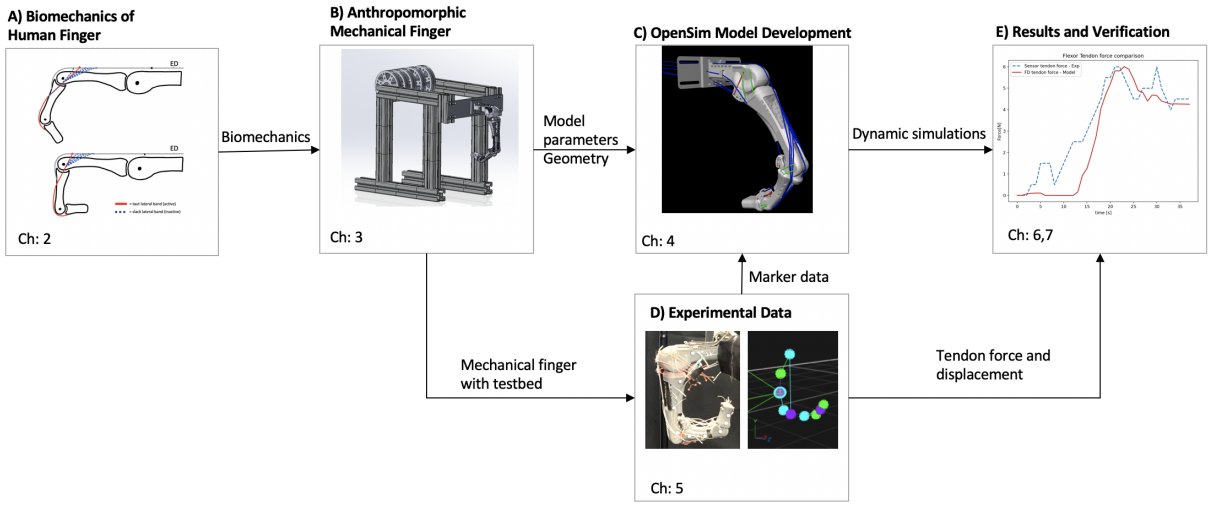

Figure 1.7: Overview of the structure of this study

2

Anatomy and Function

The human finger consists of structures compromising bones, muscles, ligaments, and joints that work together to facilitate fine motor control, gripping, and grasping capabilities. Before creating a computational musculoskeletal model, it is essential to first describe the anatomical features of the finger and understand the principles behind the IPJ coupling mechanism. This chapter provides an overview of finger anatomy and explains the key elements of the IPJ coupling, which are crucial for coordinated finger movements.

2.1. Finger Anatomy

2.1.1. Bone Structure and Joints

The terminology for the relative positions of the hand is shown in Figure 1. Each finger, except the thumb, contains three phalanges, namely the distal, middle, and proximal. There are three finger joints in each finger, from proximal to distal: metacarpophalangeal joint (MCP), proximal interphalangeal joint (PIP), and distal interphalangeal joint (DIP). Each joint allows specific movements, contributing to the finger's versatility.

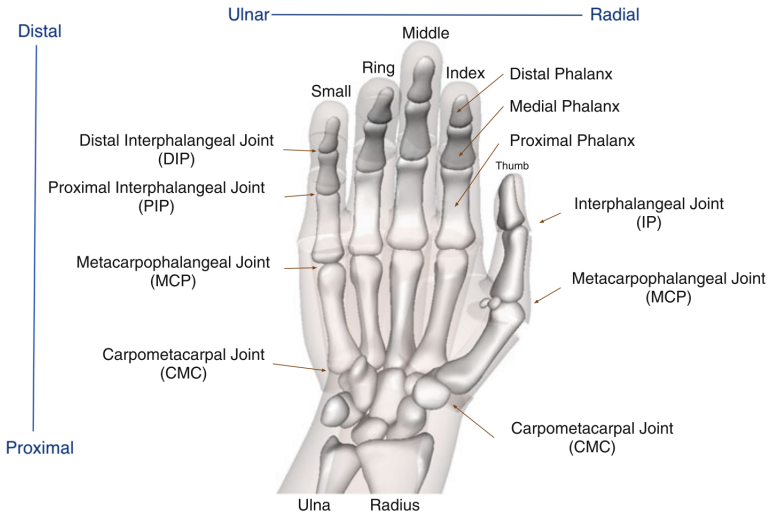

Figure 2.1: Hand anatomy and relative position definition. *Adapted from [29]*

- Metacarpophalangeal (MCP) Joint: Connects the metacarpal bone to the proximal phalanx. It is a condyloid joint, allowing for flexion-extension as well as abduction-adduction movements [24].
- Proximal Interphalangeal (PIP) Joint: Connects the proximal and middle phalanges. Its bicondylar joint provides lateral and some rotational stability, even without ligaments, allowing flexion-extension [24].
- Distal Interphalangeal (DIP) Joint: Connects the middle and distal phalanges, facilitating flexion-extension at the fingertip. Similar to PIP joint, it is a bicondylar joint [24].

2.1.2. Main Muscle-Tendons

The finger consists of an intricate tendon network for transmitting forces generated by the muscles to the finger bones, whereby tendons connect the muscles to the bones, see Figure 2.2. The finger muscles can be categorized into extrinsic and intrinsic muscles [30]. The coordination of these muscles forms the Extensor Mechanism (EM), or Extensor Apparatus (EA), which is crucial for distributing forces across the fingers. The extrinsic muscles originate from the forearm and extend into the hand and are responsible for the gross movements of the hand, these muscles are divided into two groups: flexors and extensors muscles [30] Flexor muscles pass through the palm and enable finger flexion (bend fingers), including the flexor digitorum profundus (FDP), flexion of the DIP joint, and the flexor digitorum superficialis (FDS), flexion of the PIP joint [30, 31]. Extensor muscles are located on the back of the hand and enable finger extension (straighten fingers), including extensor digitorum (ED) and extensor indicis (EI), this muscle is an extension of the ED muscle but has a separate tendon to the index finger [31]. Intrinsic muscles are located within the hand and are responsible for the precise movements of the fingers, the main two muscles located in the index finger are the lumbrical and interosseous muscles [31]. The lumbrical muscles (LUM) originate from the tendons of the FDP muscle and are inserted into the EM. These muscles are responsible for the flexion of the MCP joint and the extension of the IP joints. The interosseous muscles, the palmar interossei (PI), and the dorsal interossei muscles (DI) originate from the metacarpal bones and into the EM. These muscles are responsible for abduction-adduction of the fingers and also assist in flexion-extension, of the MCP joint [31].

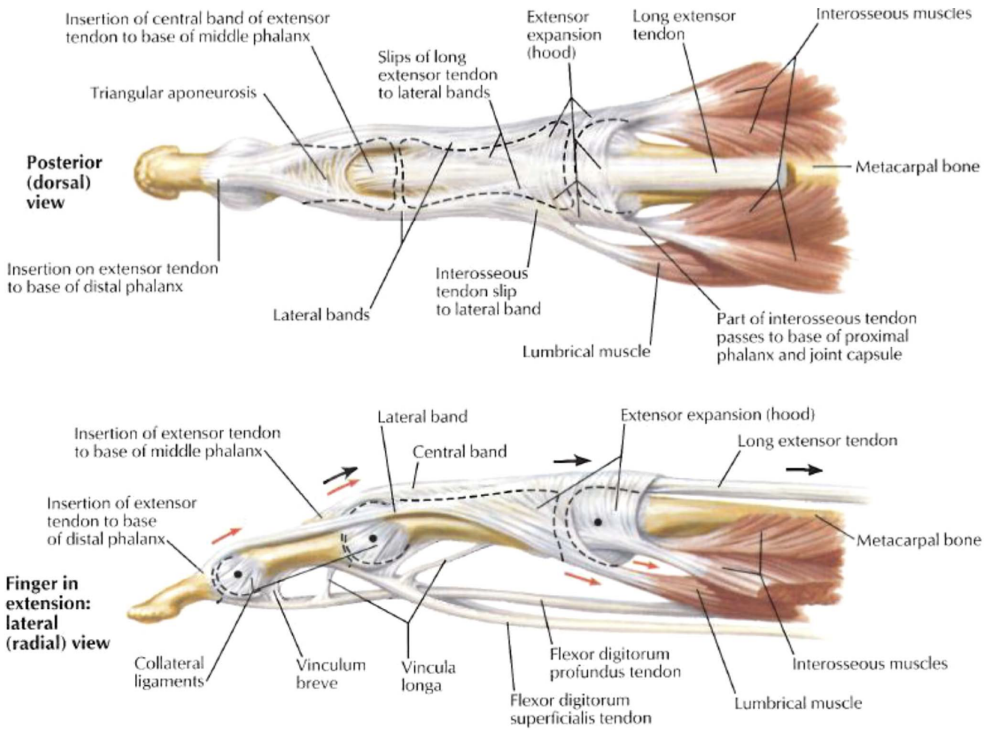

Figure 2.2: Anatomy of the Index Finger [32]. This figure shows the primary tendons involved in finger movement: the extensor digitorum (ED) for extension, the flexor digitorum profundus (FDP) for DIP joint flexion, and the flexor digitorum superficialis (FDS) for PIP joint flexion. The interosseous tendons facilitate finger abduction and adduction. Additionally, the Lateral Bands, originating from the extensor expansion, insert into the distal phalanx (coupling of distal joints). The joints are stabilized by collateral ligaments and volar plates (not highlighted in the figure).

In the presented finger model, the main tendons incorporated are those that are irredundant and correspond to an independent degree of freedom: the ED, FDS, FDP, radial interosseous (RIO), and ulnar interosseous (UIO) tendons. This approach simplifies the model and aligns with the tendons implemented in the mechanical finger.

2.1.3. Joint Ligaments

Ligaments stabilize finger joints by preventing excessive movement and maintaining joint integrity [1, 33]. The primary ligaments involved are the collateral ligaments and volar plates (palmar ligaments) [33]. Collateral ligaments, composed of interconnected collagen fibers, are located on the radial and ulnar sides of the joint. They cross the joint's axis at an angle, running from the head of the proximal bone to the front of the joint socket (see Figure 2.3). Their precise length and attachment points are essential for proper joint kinematics, ensuring the right balance of slack and tautness for full range of joint motion. The volar plates are dense fibro cartilaginous structures on the palmar side of the joint. They limit hyperextension and increase moment arm during flexion at the joints, as the flexor tendon pulleys are attached to the volar plates. Lastly, the oblique retinacular ligament (ORL), also known as Landsmeer's ligament, originates at the proximal phalanx, crosses the proximal interphalangeal (PIP) joint, and inserts dorsally at the distal phalanx. According to Landsmeer's theory, the ORL links the motion of the interphalangeal (IP) joints, ensuring that extension at the PIP joint leads to extension at the distal interphalangeal (DIP) joint, thereby preventing the DIP joint from flexing when the PIP joint is extended [34].

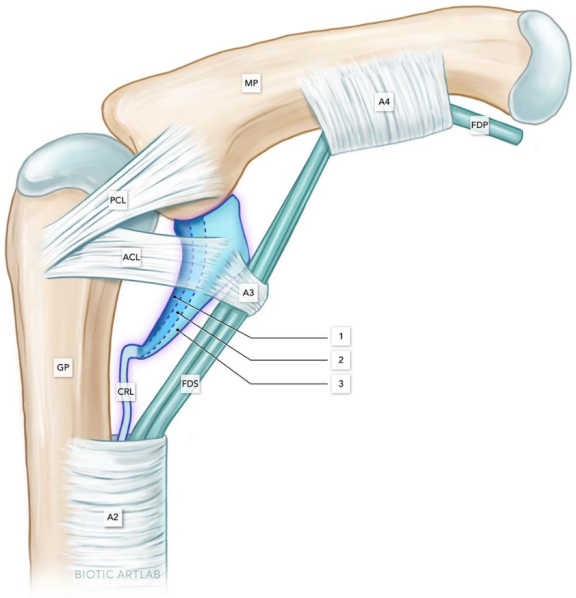

Figure 2.3: Joint ligaments and pulleys at the PIP joint. proper collateral ligament (PCL), accessory collateral ligament(ACL), (1-3) Volar plate, (A2-A4) pulleys, flexor tendons (FDS and FDP) [35]

2.1.4. Pulley System and Support Ligaments

The (annular) pulleys (A1-A2) are fibrous structures on the palmar side of the finger that keep the flexor tendons in their anatomical position during movement, shown in Figure 2.3 at the PIP joint. Three pulleys are attached to the volar plate (A1, A3, and A5), which change orientation during finger extension and flexion. Pulleys are essential for transmitting flexor tendon force through the finger [35]. If the pulleys rupture, bowstringing occurs, which can lead to a loss of strength or range of motion due to an increase in the moment arm (see Figure 2.4). The cruciate pulleys (C1-C3) are not covered in this thesis. The finger also contains other supportive ligaments: the sagittal band, transverse retinacular ligament (TRL), and triangular ligament (TL). The sagittal band, originating from the volar plate, holds the ED tendon in place over its rounded head during finger flexion, also preventing bowstringing of the ED tendon. The TRL, located on the radial and ulnar sides of the PIP joint, stabilizes the Lateral Bands during PIP extension, keeping them aligned at the sides of the joint. The TL, found at the middle phalanx, keeps the Lateral Bands from separating during finger flexion.

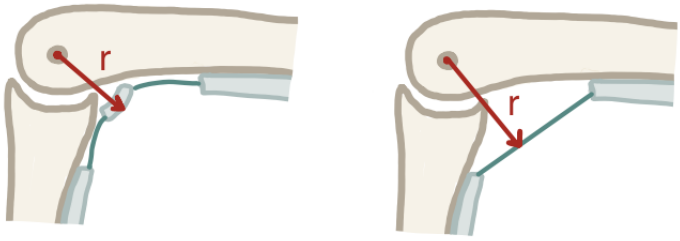

Figure 2.4: Flexor bowstringing without A3 pulley, increasing moment arm, r

2.2. IPJ Coupling Mechanism

The interphalangeal joint (IPJ) coupling mechanism is an important part of the Extensor Mechanism, primarily facilitated by the Lateral Bands formed from the ED tendon. These Lateral Bands are responsible for coordinating of the interphalangeal (IP) joints, PIP and DIP joints, ensuring that the movement of one joint influences the others. The ED tendon inserts at the middle phalanx, generating torque at the PIP joint and enabling MCP and PIP joint extension. The Lateral Bands, originating from the ED tendon, encircle the PIP joint and insert on the dorsal side of the distal phalanx, where they extend to the DIP joint [27].

As demonstrated in a cadaveric study by Leijnse et al. (2010), this coupling is evident in the relationship between the PIP and DIP joint angles during flexion and hyperextension [36]. As the PIP joint flexes, the ED tendon moves distally, creating slack in the Lateral Bands and allowing the DIP joint to flex [27].
Leijnse and Spoor (2012) assessed the function of individual strands of the Lateral Band using a 2D kinematic model of the extensor apparatus (EA). Multiple strings were used to represent the Lateral Bands and simulate the IPJ coupling mechanism, demonstrated in Figure 2.5). In finger extension, the moment arm of the Lateral Band (LB_1) is proportional to the ED tendon, keeping the Lateral Band taut and maintaining DIP joint extension. As the finger flexes, the Lateral Band shifts palmarly lateral at the PIP joint, reducing the moment arm and creating slack, which decreases tension in the Lateral Band, allowing DIP joint flexion. This process continues as each Lateral Band becomes taut and slackens with flexion. This multi-string approach captures the complex, interdependent movements of the joints, accurately representing the IPJ coupling mechanism in simulations. However, the precise attachment points and lengths of the Lateral Bands are important for achieving accurate IPJ coupled trajectories. This IPJ coupling mechanism is implemented in both the anthropomorphic mechanical finger, as established in previous work, and in the development of the OpenSim model.

2.3. Conclusion

This chapter provided a comprehensive overview of the biomechanics of the human finger, focusing on its anatomical structures, including bones, joints, muscles, tendons, ligaments, and the intricate pulley system. A key focus was the interphalangeal joint (IPJ) coupling mechanism, facilitated by the Lateral Bands of the extensor digitorum (ED) tendon, and is essential for coordinating the movement between the proximal and distal interphalangeal joints and the force distribution during IPJ-flexion. The insights gained from this analysis will be applied in the anthropomorphic mechanical finger (Chapter 3) and further utilized in the development of the OpenSim model (Chapter 4) for simulating finger movements.

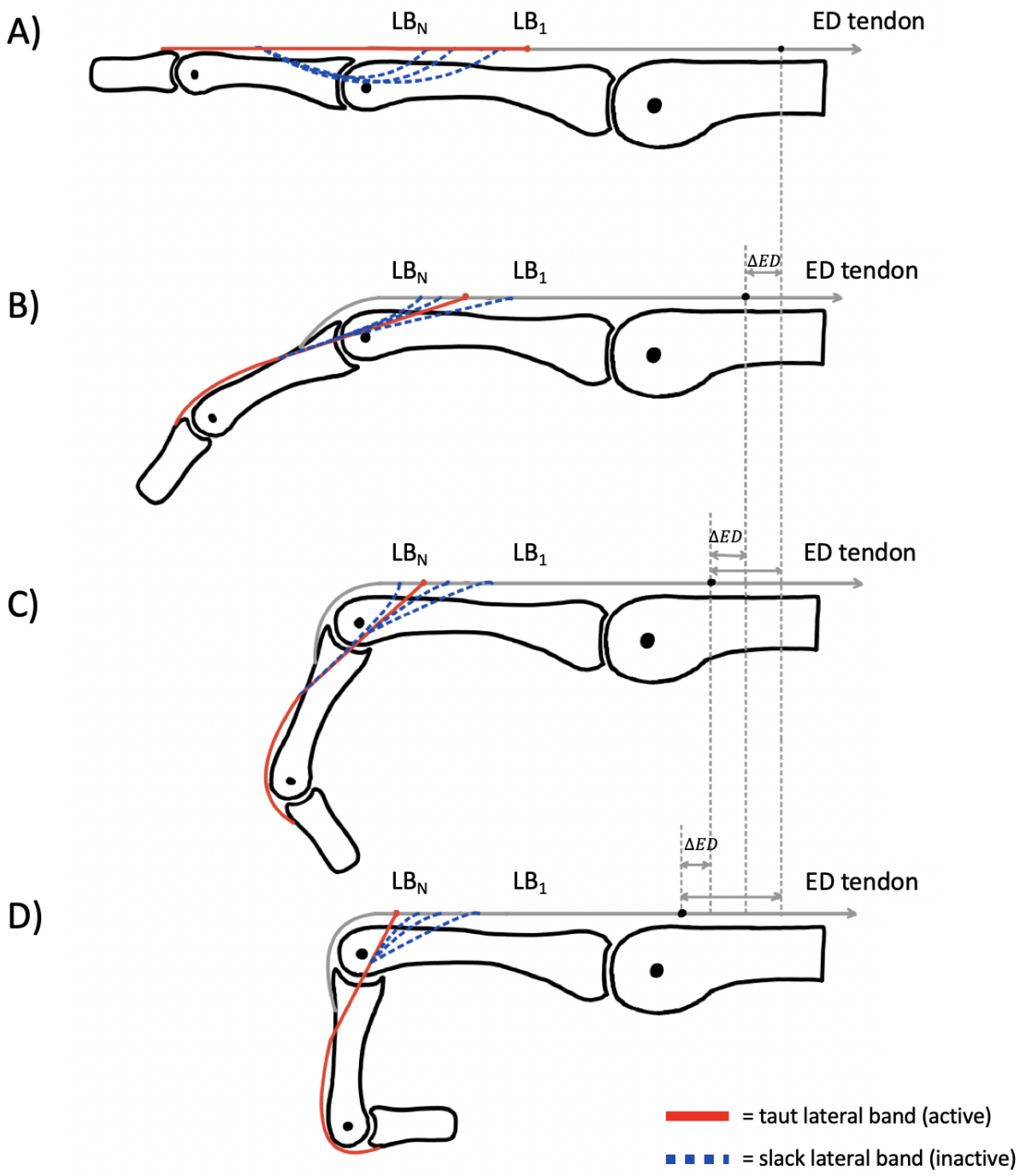

Figure 2.5: IPJ coupling mechanism. (A) The most proximal Lateral Band (LB_1) remains under tension, maintaining DIP joint extension as its moment arm is proportional to the ED tendon. (B) As IPJ flexion begins, the ED tendon shifts distally, causing LB_1 to move palmarly lateral at the PIP joint. This reduces the moment arm, creates slack in LB_1, and allows DIP joint flexion, transferring tension to the next Lateral Band. (B-D) This transfer of tension of the Lateral Bands continues as IPJ-flexion goes on, whereby the previous lateralband (LB_{N-1}) slackens and next lateralband become taut (LB_N) during IPJ flexion . *Adapted from Leijnse and Spoor (2012) [13]*

3

Anthropomorphic Mechanical Finger

This chapter describes the development of the anthropomorphic mechanical finger used for this research project, which replicates the functional and anatomical characteristics of a human finger through incorporating anthropomorphic joints and ligament systems. Any adjustments that have been made from the previous work and will specifically be highlighted in the respective sections.

3.1. Skeleton

To verify the simulation model through experiments, a new version of the anthropomorphic mechanical finger was developed, see Figure 3.1, based on the previous project [24].

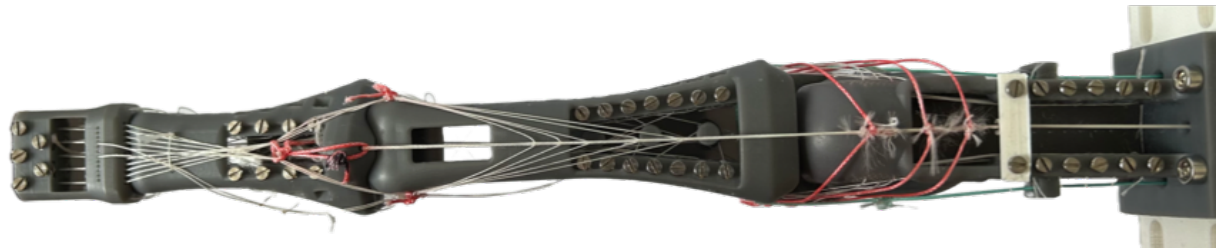

(a) Topview

(b) Sideview

Figure 3.1: Overview of the mechanical finger (Finger scale 2:1)

The main difference was the scale: while the previous finger was at a 5:1 scale, the new finger has been scaled down to a 2:1 ratio.This scale reduction decreases the overall weight by a factor of the original weight*S^{-3}, which impacts the force exerted on the finger tendons and the force required for actuation. In addition, frame size and space requirements have been reduced, leading to more efficient material use. Each CAD part has been linearly scaled down, with modifications made to the fixation method. The dimension of the finger is given in Table 3.2, with Figure 3.3.

Dimension of the mechanical finger (mm)	
Metacarpal Length	75
Proximal phalanx Length	87.59
Middle phalanx Length	53.64
Distal phalanx Length	25.31
MCP joint (r_x x r_y x r_z)	16.66 x 14.5 x 20
PIP joint (r_x x r_y x r_z)	7.43 x 8.2 x 18.01
DIP joint (r_x x r_y x r_z)	6 x 6.62 x 16.4

Figure 3.2: Bone segment dimensions of the mechanical finger

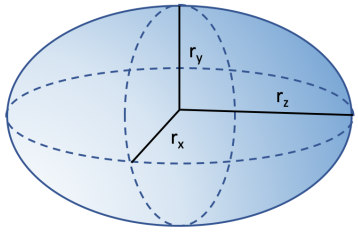

Figure 3.3: Reference for joint dimensions

A new attachment system was developed to improve the connection of strings to the components. Previously, strings were fixed to the phalanges using guides with fixing screws, but with the smaller scale and different material of the new model, repeated unscrewing and re-screwing could potentially damage the surrounding material over time. To address this, a nut-and-screw system was introduced to prevent material degradation during adjustments. A small slot was created to house a 1.7 mm nut, allowing a screw to be securely fixed on top. Beneath this slot, a small hole was made for inserting a nylon string, as shown in Figure 3.4. This design ensures that the material remains intact during repeated adjustments and allows for easy removal and reconfiguration of strings. The CAD design was adjusted to incorporate these changes while preserving the outer dimensions and shape, ensuring that the new model maintains the correct form and functionality of the previous design.

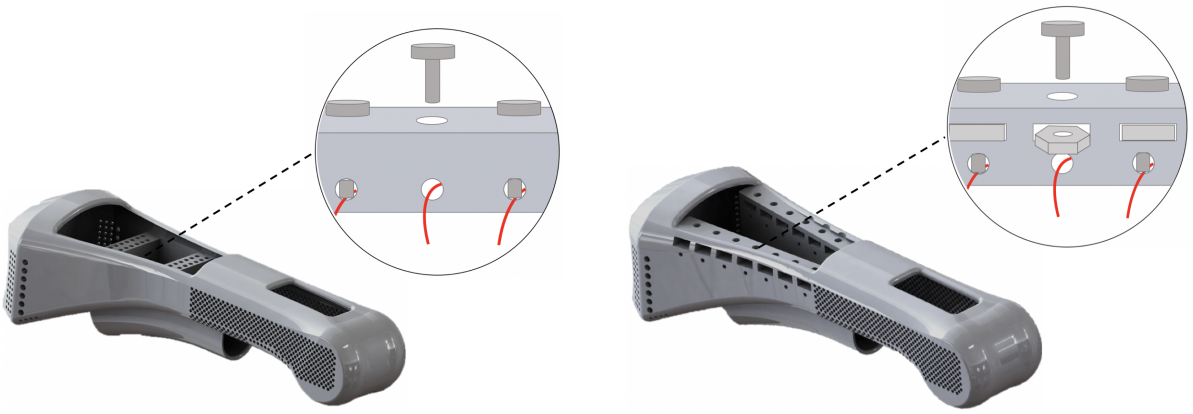

(a) former design using only screw fixations **(b)** new design which include nut and screw fixations

Figure 3.4: CAD model of the proximal phalanx

The mechanical model employs SLA (Stereolithography) printing technology instead of the previous PLA filament method. The reduced dimensions posed challenges in accurately creating tiny holes and intricate details with PLA using the available printer. SLA printing technology addresses these issues by enabling the production of smaller parts with finer details and more precise holes. This is achieved by curing liquid resin into three-dimensional objects using a light source. The segments were printed in the sagittal plane to ensure minimal filling of the holes during printing. The draft resin used is three to four times faster than parts printed with other standard resins. Scaled-down and produced using the Formlabs Form 3 printer, the SLA material remains strong enough to withstand the forces acting on the finger model during motion. Furthermore, SLA printing produces much smoother joint surfaces, which were then sanded with progressively finer grits of 400, 600, 1000, 1200, and 2000 to achieve a refined finish, eliminating the need for additional coating.

3.2. Joints

The joints of the mechanical finger are created using the head and socket geometry of the joint, allowing the components to slide over each other. The head and socket were designed so that the MCP joint could perform both flexion-extension and abduction-adduction, while the PIP and DIP joints were restricted to flexion-extension. Collateral ligaments were used to constrain the range of motion and stabilize the joints. As described in Chapter 2, the collateral ligaments become taut at specific joint angles, thereby contributing to the range of motion, see Figure 3.5. The volar plates were designed to match the shape of the joints, incorporate flexor pulleys, and are attached with string to the bones, preventing hyperextension and ensuring stability.

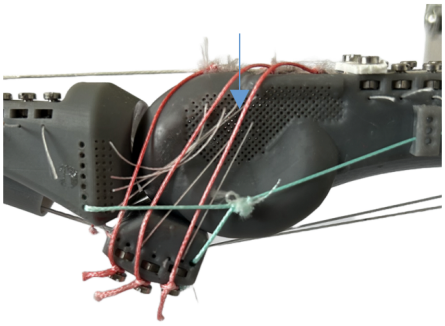

(a) Most right ligament is taut others are slack at MCP joint extension

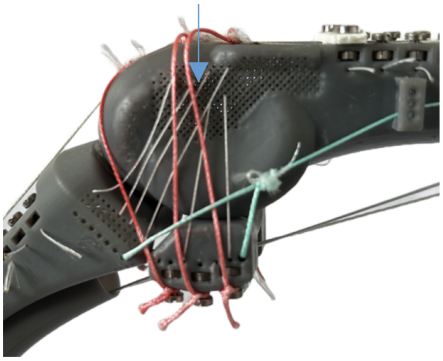

(b) Middle ligaments become taut during mid MCP joint flexion

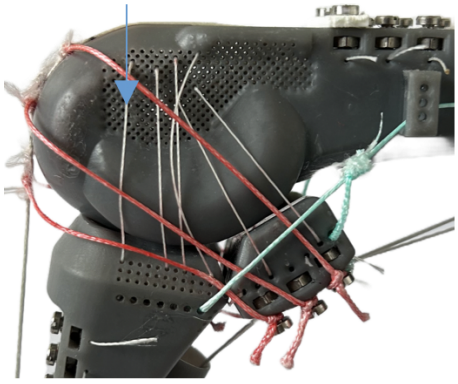

(c) Most left ligament and volarplate string are taut other ligaments become slack at almost full MCP joint flexion

Figure 3.5: Collateral ligaments become taut and slack during MCP joint flexion

3.3. Tendon Paths

The mechanical finger incorporates the following tendons: the extensor digitorum communis (ED), flexor digitorum superficialis (FDS), flexor digitorum profundus (FDP), and the interosseous (IO) tendons. A combination of Dyneema and nylon strings as tendons and ligaments. Dyneema strings, known for their non-elasticity and low friction, are used for the tendons, as in the previous model. Although the number of attachment strings remains unchanged, the smaller scale required the use of nylon strings instead of Dyneema to attach the extensor mechanism, volar plates, and ligaments due to space constraints and the thickness of available Dyneema strings. Stiff nylon strings were selected for their similarity to the stiffness range of human tendons, as demonstrated in [24]. The Lateral Bands, which originate from the ED tendon, that ensure IP-coupling are arranged as described in Chapter 2 and applied similarly to the method described in the previous model. The load of the tendons is transferred over the range of motion of

IP flexion, which is determined by correctly adjusting the length so that each band becomes taut at specific joint angles, see Figure 3.6. In Appendix A the top view of the IPJ coupling is given.

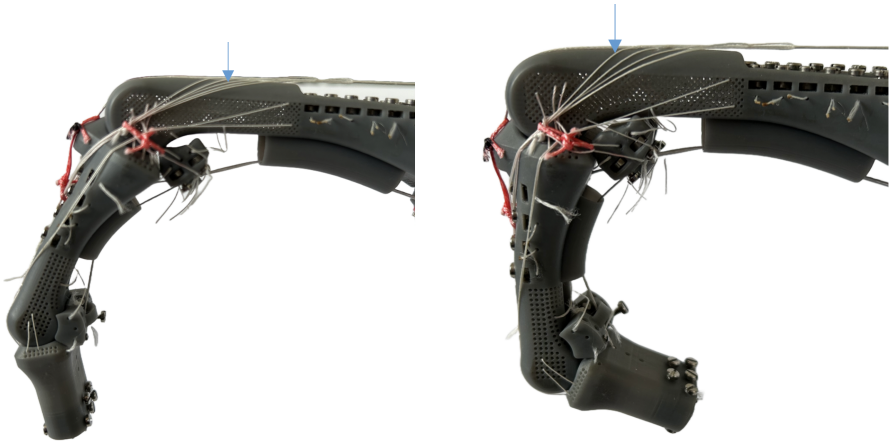

(a) Proximal lateralbands are slack as the middle lateralbands become taut

(b) Middle lateralbands are slack as the distal lateralbands become taut

Figure 3.6: IPJ coupling mechanism, Lateral Band tension distribution during finger flexion in the mechanical finger

3.4. Actuation of the Tendons

To perform experiments, a support frame was constructed to mount the mechanical finger, see Figure 3.7. This frame, built from 30 mm x 30 mm aluminum profiles, was chosen for its ease of adjustment and future modification capabilities. These profiles allow for the easy addition of components, such as actuators or sensors, by adjusting the height and width. After constructing the frame, a laser-cut aluminum plate was used to mount the robotic finger. This plate had holes through which the tendons were threaded. The plate was then mounted on the frame, with the tendons connected to the finger and extending to a pulley lever system on the opposite side. To ensure the tendons remain in tension, a lightweight was applied at the end of the pulley. This setup allows for manual adjustment of tendon positions to achieve the desired finger motions. The pulley lever system was designed with a roller bearing in its center hole to ensure smooth operation. For future experiments, the applied masses will be adjusted as detailed in Chapter X. This assembly setup ensures a stable and adaptable platform for conducting various experiments, providing the flexibility to modify the system as needed.

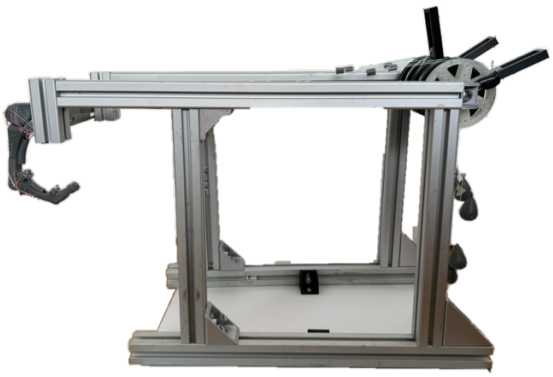

Figure 3.7: Setup of the mechanical finger attached on frame with a pulley lever system to actuate the tendons (weight added at the end of the tendons)

3.5. Conclusion

This chapter described the development of the anthropomorphic mechanical finger specifically designed for the experimentation and verification of simulation models. The mechanical finger is capable of replicating the functional movements of a human finger, including flexion-extension and abduction-adduction at the MCP joint, and flexion-extension at the PIP and DIP joints. It integrates the anatomical joints with collateral ligaments and volar plates that replicate natural stabilization and range of motion. Tendons and ligaments made from Dyneema and nylon strings are arranged to ensure accurate IPJ coupling. This mechanical finger will be utilized to develop the OpenSim model (Chapter 4), providing a physical counterpart for testing and verification (Chapter 5).

4

Opensim Model Development

This chapter details the development of an OpenSim model designed to simulate an anthropomorphic mechanical finger. It describes the creation of the model using OpenSim Creator [37], including the integration of nine rigid bodies and anatomical joints to accurately replicate finger kinematics and dynamics. The chapter also discusses the modeling of tendons and the IPJ coupling mechanism, as well as how the model was adapted for verification through comparison with experimental data. This overview provides an understanding of the model's development and its application in simulating finger movements.

4.1. Overview Opensim Model

The simulation model is developed using OpenSim Creator, a standalone UI and open-source software for creating, editing, and simulating OpenSim models. The model compromises a set of nine rigid bodies: the metacarpal, proximal phalanx, middle phalanx, distal phalanx, three volar plates, and an attachment plate where the metacarpal bone connects. Bone geometries are derived from separate CAD files created in SolidWorks, which serve both visualization purposes and guide the placement of tendons, joints, and other model components. Key model parameters, such as the center of mass (COM) and inertia around the COM, are also determined through SolidWorks. The masses of the bones and volar plates are measured using a scale, and these measurements are subsequently used to update the inertia values. The overview of the complete OpenSim model is shown in Figure 4.1

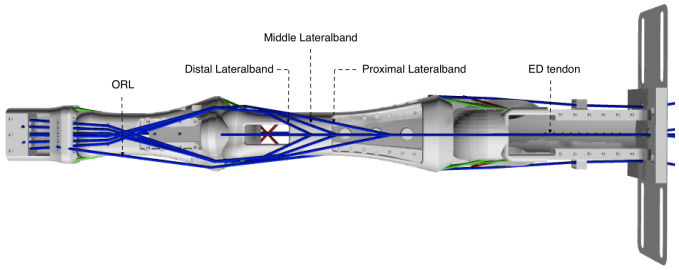

(a) Topview

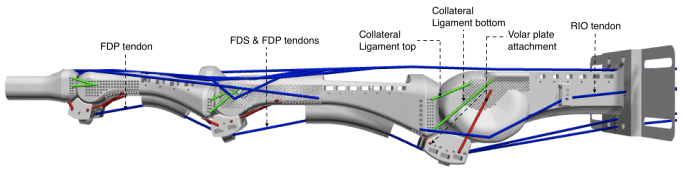

(b) Sideview

Figure 4.1: Overview of the OpenSim model. The model consists of four bodies, each represented by bone geometry meshes that help define the paths of tendons and ligaments. These bodies are connected via joints. The model includes the primary tendons (ED, FDS, FDP, RIO, UIO) and Lateral Bands (blue). Collateral ligaments (green) and volar plate attachments (red) are present at each joint, on both the ulnar and radial sides.

4.2. Joint Kinematics

4.2.1. Modeling of MCP, PIP, and DIP Joints

The rigid bodies in the model are interconnected through joints that establish the kinematic relationships between each body, thereby defining the movement of the child's body relative to its parent body (Figure 4.2) [38].

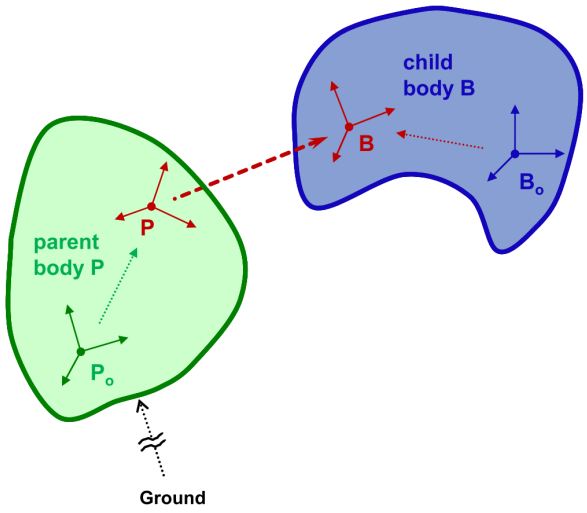

Figure 4.2: Joint defined between two bodies (Parent (P) and child (B) frame) [38]

The metacarpophalangeal (MCP), proximal interphalangeal (PIP), and distal interphalangeal (DIP) joints are modeled using ellipsoid joints to represent the complex articulations of these joints. The ellipsoid joints allows rotation and translation along the surface of an ellipsoid fixed the parent [39]. Unlike ball-and-socket or hinge joints, which constrain movement to a rotation with a constant radius, the ellipsoid joint can be customized to allow the socket to move over the surface semi-spherical shapes of the bone head, better following the natural articulation of these joints as the traces the curvature of the joint more closely, see schematic representation in Figure 4.3.

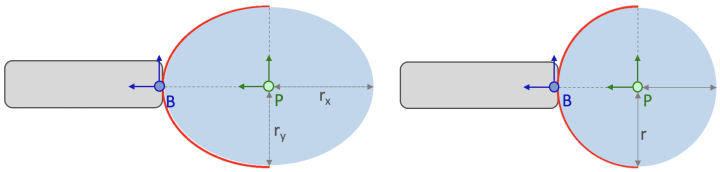

Figure 4.3: Schematic representation of an ellipsoid joint (with varying radii rx/ry) compared to a hinge or ball-and-socket joint (with a constant radius r). In both cases, the child body (B) follows the curvature of the joint (red). In the ellipsoid joint, body B follows a path with a changing radius, while in the hinge or ball-and-socket joint, the curvature remains consistent with a constant radius.

The MCP joints are characterized by two degrees of freedom, allowing for both flexion-extension and abduction-adduction movements, with the possibility to include axial rotation, which is not included in this thesis. In Figure 4.4, the MCP joint in the model is seen with its joint ligaments using an ellipsoid joint. In contrast, the PIP and DIP joints are constrained to a single degree of freedom, permitting only flexion-extension movements, as for these joints the bone shape provides for lateral and some axial-rotational stability, even without ligaments [24], as a result these joints were locked to only move in flexion-extension. This modeling approach effectively captures the essential kinematics of the joints while maintaining computational efficiency.

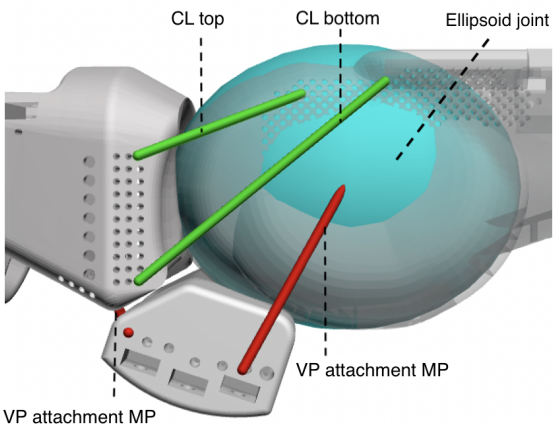

Figure 4.4: MCP joint in the model utilizing an ellipsoid joint. The ellipsoid joint is fixed at the head of the metacarpal(MP) (transparent) and the socket of the proximal phalangeal (PP) traces the surfaces of the ellipsoid (blue). Collateral ligament (CL) and volar plate (VP) are fixed at the metacarpal (MP) and proximal phalangeal (PP)

4.2.2. PathSpring Objects for Ligaments and Volar Plates

To constrain and therefore limit the range of motion of the joints, collateral ligaments and volar plates were added. These structures were modeled as PathSpring objects, a massless Force element that mimics the behavior of the strings used in the mechanical finger. The closest Force element that mimics the physical strings is the PathSpring, which applies tension along a path connected to the bodies, with the paths for the ligaments and volar plates defined by the origin and insertion points of the mechanical finger.

The PathSpring is characterized by its linear stiffness (K), dissipation (D) parameters, and resting length (l_0). The tension force is calculated based on the amount of stretch beyond its resting length:

$$Tension = (K \cdot s) \cdot (1 + D \cdot \dot{l})$$

where $s = l - l_0$, for, $l < l_0$ the tension between the bodies is zero, and the PathSpring is considered slack. The linear stiffness of the Dyneema string and nylon string used in the model are approximately 25 kN/m and 1.3 kN/m, respectively. These values were determined by conducting a simple force and displacement experiment, where the strings were pulled with a force sensor to measure displacement. To dampen the motion and prevent oscillations (since PathSprings are used as elements and no friction element was added), a damping element was integrated into the joints. A small rotational damping was added to the joints to reduce overall oscillatory movement, ensuring smoother and more controlled joint motion.

Collateral Ligaments

Each joint consists of two collateral ligaments on either side. The range of motion was determined by setting their rest lengths at two specific joint angles: finger extension and flexion. One ligament, the bottom ligament, has its rest length set at joint extension. This ligament gradually becomes taut during finger flexion and slowly becomes slack as flexion progresses. The other ligament, the top ligament, initially starts in slack and has its rest length set at the end of joint flexion (90 degrees). This ligament becomes taut if the joint exceeds this flexion angle, see Figure 4.5 with its corresponding graph in Figure 4.6.

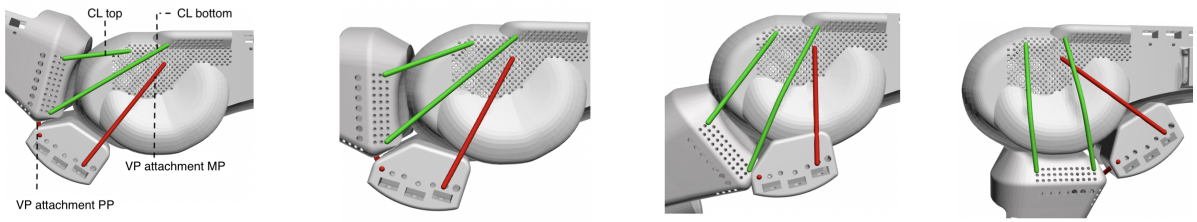

(a) VP attachment are taut in MCP joint hyperextension, CL slack

(b) CL bottom is taut and VP become slighty slack in MCP joint extension

(c) CL bottom is taut but get slacker as MCP joint goes to mid flexion to full flexion

(d) CL top is taut and VP starts getting taut at MCP joint full flexion

Figure 4.5: Collateral ligament (CL) and volar plate (VP) attachment at the metacarpal(MP) and proximal phalangeal (PP) become taut and slack during MCP joint hyperextension to flexion, with corresponding graph in Figure 4.6

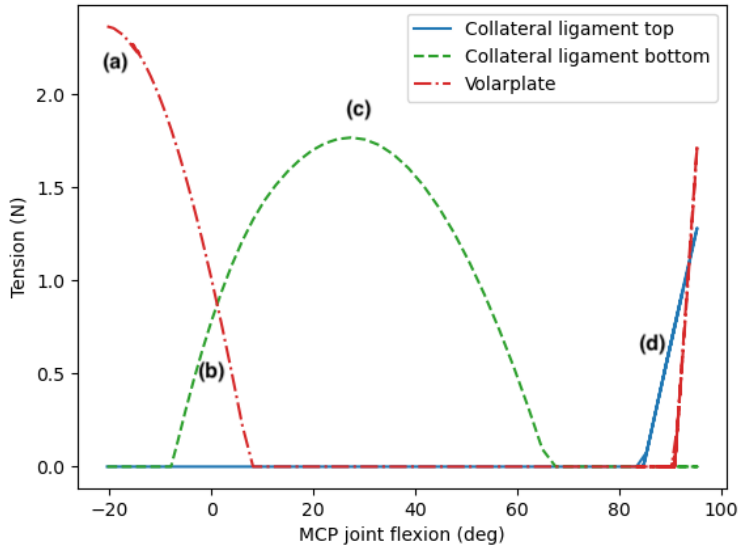

Figure 4.6: Tension of the collateral ligaments and volar plates during MCP joint extension-flexion, with corresponding positions in Figure 4.5

Volar Plates

The volar plate exhibits both rotational and translational movement and tends to displace proximally toward the bone to which it is attached (see Figure 4.7), ellipsoid joints were found to be unsuitable. Instead, a custom joint was created using a spline function and a constraint that ties the volar plate's movement to the joint's coordinates. This approach enables precise positioning of the volar plate at various joint angles, with the plate's coordinates being dependent on these angles.

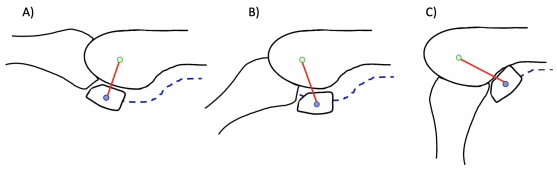

Figure 4.7: Volar plate motion during finger MCP joint flexion. (A-C) Volar plate follows a path that ensures that it rotates and translates at specific joint extension-flexion angles. The volar plate path is defined in the simulation model with a spline function (blue dotted line) and is constrained to move with the MCP joint (red line)

This custom joint was specifically designed to model the function of the volar plate: preventing hyperextension. To achieve this, the volar plate was linked to PathSprings that tighten during hyperextension. The rest lengths of these PathSprings are set at joint extension (0 degrees) and become taut when hyperextension occurs, applying tension to control and limit the joint's hyperextension, see Figure4.6.

4.3. Tendons, Extensor mechanism

4.3.1. Main tendons

The simulation model incorporates the same tendons as the mechanical finger: ED, FDS, FDP, and the IO tendons. These tendons are modeled as PathSprings, similar to the ligaments and volar plates. The tendon paths in the model play a crucial role in determining the moment arm by defining the geometric routing of the tendons, as OpenSim calculates this by using the defined path and wrapping surfaces. The insertion points are positioned as accurately as possible to match those of the mechanical finger, ensuring that the model closely replicates the mechanical finger.

For the extensor tendons, fixed points (via points) and wrapping surfaces are strategically placed to prevent bowstringing and ensure that the tendons follow a realistic path over the joints. To accurately route the tendon paths around the joints, various wrapping objects are used:

- **Ellipsoid Wraps:** These are placed at the MCP and PIP joints to manage flexion-extension and MCP abduction-adduction. The ellipsoids are shaped and positioned to align with the head of the bone, the joint's center of rotation, similar to the ellipsoid joints. This ensures that the ED tendon wraps around the bone head, which is critical for maintaining the correct moment arm.
- **Cylinder Wraps:** At the DIP joint, two wrap cylinders are placed. One cylinder manages the flexors (limited to wrap on the anterior side), while the other manages the extensors (limited to wrap on the posterior side. The use of quadrants ensures the path remains in a designated direction, preventing the path from looping under the object at certain angles.

The geometric path of the flexor tendons (FDS and FDP) is primarily defined by via points. These via points are aligned with the locations of the pulleys in the finger, which play a crucial role in preventing bowstringing at the joints. By fixing the tendon paths at these pulley locations, the model ensures that the flexor tendons maintain a close relationship with the bones, reducing the risk of bowstringing during flexion and maintaining consistent moment arms throughout the range of motion.

4.3.2. Extensor Mechanism

The model includes three separate Lateral Bands on each side of the ED tendon: proximal, middle, and distal (Figure 4.8 and 4.1). The Lateral Bands follow the same path as the ED tendon by sharing the same via-points, similar done in other OpenSim model [15]. Thus, the displacement of the ED tendon directly influences the tautness and slackness of the Lateral Bands.

- **Proximal Lateral Bands:** These bands mimic the function of the Lateral Bands that facilitate DIP joint extension when the ED tendon is pulled. They need to be taut when the PIP joint is extended (finger in extension) and slack when the PIP joint flexes.
- **Middle Lateral Bands:** These bands manage IPJ flexion by remaining slack when the finger is extended (PIP extended) and becoming taut during mid-range PIP and DIP flexion, with their tautness decreasing as flexion progresses.
- **Distal Lateral Bands:** These bands are slack in extension but become taut as IPJ flexion nears completion.

Correct adjustment of the slack lengths for these bands ensures that they become taut at the appropriate stages of IPJ flexion, thereby achieving accurate IPJ coupling. The stiffness of the ED tendon and the Lateral Bands is adjusted to ensure that the overall stiffness does not exceed 25 kN.

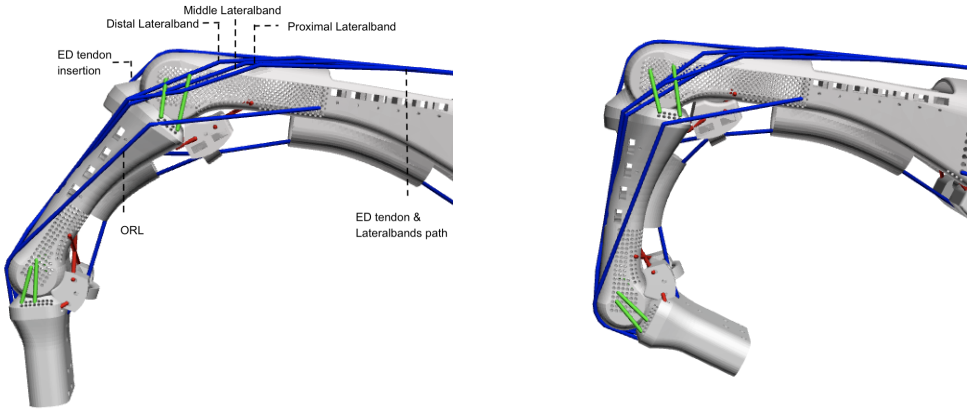

(a) Proximal lateralbansd are slack and the middle lateralbands are taut

(b) Middle lateralbands are slack and the distal lateralbands are taut

Figure 4.8: IPJ coupling mechanism and Lateral Band tension distribution during finger flexion in the simulation model. During finger extension, the proximal Lateral Band remains taut, ensuring DIP joint extension. As the IPJ flexes, the proximal Lateral Band slackens, while the other Lateral Bands become taut, depending on the degree of IPJ flexion

4.4. OpenSim Model Test Environment

For the kinetic simulation, the OpenSim model was adapted by attaching weights to the ends of the tendons, simulating the tendon actuation of the mechanical finger (see Figure 4.9). These weights were modeled as bodies connected through slider joints, allowing only sliding motion. In the Forward Dynamics simulation, tendon displacement was specified as an input through prescribed motion rather than being influenced by the weight's mass. This means that the mass of the weights did not affect the simulation; instead, the tendon displacement was determined solely by the prescribed motion of the weights. Thus, while the weights were modeled as bodies within the simulation, their mass was effectively neglected, and the tendon length changes were driven by the predefined weight displacement.

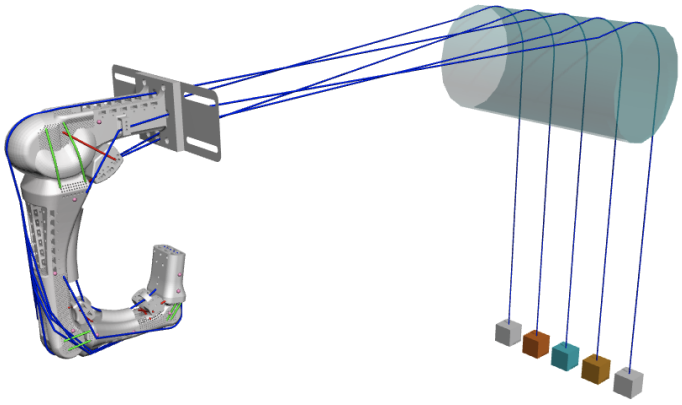

Figure 4.9: OpenSim model with weights added at the end of the tendon; The simulation input is the weight displacement at each time step used in the Forward Dynamics (FD) simulation

The initial joint positions, obtained from inverse kinematics, served as the starting point for the simulation. To ensure accurate simulation conditions, the resting lengths of the tendons were adjusted to maintain neutral tension at the start of the simulation. In the mechanical finger setup, adjusting the finger's position (e.g., during flexion) naturally causes the weights at the end of the tendons to move, similar to a seesaw effect. However, in the simulation model, changing the initial finger position to match the joint positions obtained from inverse kinematics does not cause the weights to shift—they remain fixed. This discrepancy

could create either slack or excessive tension in the tendons. To address this, the tendons' resting lengths were adjusted based on the lengths that would result at that specific finger position, ensuring they were in a neutral tension. This meant that the tendons were neither slack nor overly taut, corresponding to the natural resting length they would have at that joint position, thereby maintaining realistic tension at the start of the simulation. Similarly, in the model, the Lateral Bands follow the same path as the ED tendon and connect to the weight, meaning they are also affected by changes in the finger's initial position. Although the Lateral Bands are anatomically fixed, in the simulation, they are not directly attached to the ED tendon, which allows for adjustments. As a result, their lengths were adjusted on a per-experiment basis, using trial and error to account for variations and ensure proper tension during specific phases of IPJ flexion.

4.5. Conclusion

This chapter detailed the development and implementation of the OpenSim model for simulating the anthropomorphic mechanical finger. Utilizing OpenSim Creator, the model incorporates nine rigid bodies and advanced joint kinematics to accurately replicate human finger movements. Anatomical joints are modeled using ellipsoid joints, which facilitate both translation and rotation, alongside the incorporation of joint ligaments. PathSprings are utilized to accurately simulate the behavior of ligaments and volar plates, ensuring proper joint constraints. Tendon paths, including those for the extensor and flexor tendons, are carefully defined to prevent bowstringing. The integration of weights and their displacement adjustments in the model allows for the simulation of real-world conditions and enables the verification of the model's performance against the physical mechanical finger (Chapter 5).

5

Method and Experimentation

To verify the accuracy of the OpenSim model, a series of experiments were conducted to compare the model's behavior with that of a mechanical finger. These experiments focused on finger flexion under load, utilizing motion capture data, inverse kinematics (IK), and forward dynamics (FD) to assess the model's performance.

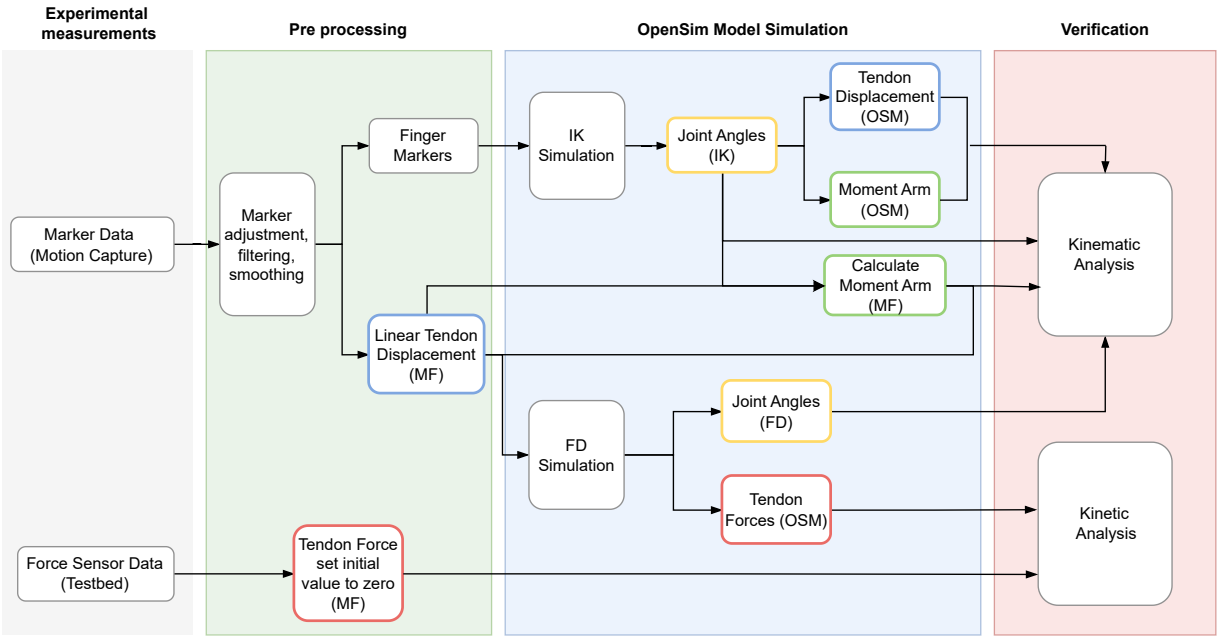

Figure 5.1: Overview of the methodology used to evaluate the performance of the musculoskeletal OpenSim model (OSM) against the anthropomorphic mechanical finger (MF). The verification will involve the results from the experimental data, inverse kinematics (IK) and forward dynamics (FD) simulations

5.1. Experimental Design and Setup

5.1.1. Overview of Experimental Setup

An experimental setup was designed to capture the motion and forces in the mechanical finger during flexion. Experiments were performed using a motion capture system consisting of six Motive Optitrack cameras operating at 120 frames per second. The mechanical finger was securely fixed on a rigid table to minimize disturbances and small passive reflective markers were placed on the finger, shown in Figure 5.2. To obtain the tendon displacement, markers were placed on a small rigid block attached to the tendons.

Figure 5.2: Reflective markers on mechanical finger

To maximize data accuracy, all cameras were strategically positioned to capture as many markers as possible. To prevent missing any markers, the camera arrangement ensured that at least three cameras captured the finger markers and at least three others captured the tendon markers. The setup was calibrated to achieve the optimal results, which is based on the mean ray error, error in tracking the 3D position of the markers, and the mean wand error, error between the known length of the wand and the detected length. Reflective surfaces were covered to prevent interference, ensuring accurate data capture. Data processing, including marker labeling, 3D marker location extraction, missing marker correction, and data filtering, was conducted using the Motive software (NaturalPoint Inc., Corvallis, Oregon, USA).

Finger actuation was performed using a test bed equipped with a sliding platform, controlled by rotating a turning wheel. A single flexor tendon was attached to the testbed, and the turning wheel was slowly rotated to achieve the desired flexion (see Figure 5.3). Different weights were attached to the tendon to vary the load depending on the experiment. In Appendix B, the complete motion capture is depicted.

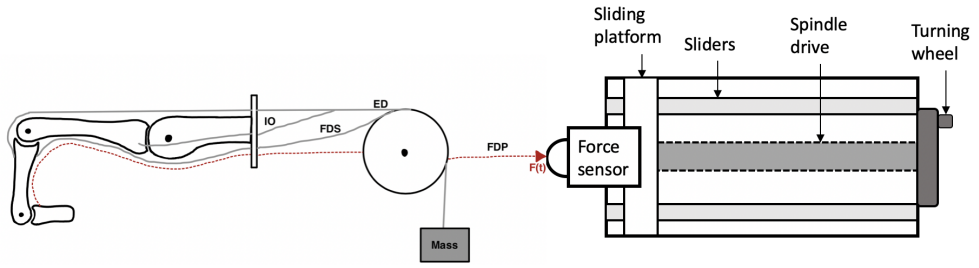

Figure 5.3: Test setup of the mechanical finger with testbed, flexor tendon attached to the force sensor with sliding platform

5.1.2. Experiments Performed

Two experiments were conducted to assess the model's ability to replicate the IPJ coupling mechanism and overall kinematics of the finger. The experiments performed were:

- Full Flexion: Flexion of the MCP, PIP, and DIP joints, the mechanical finger was initially set to a neutral position (all joints at approximately 0 degrees).
- IPJ Flexion: Flexion of only the DIP and PIP joints, with a heavy load applied to the ED tendon to keep the MCP joint as stationary as possible. The MCP joint was slightly hyperextended to prevent it from flexing when a load was applied to the flexors.

The load applied at each of the tendons is given in Table 5.1, whereby the FDP tendon was attached at the testbed, applying force during joint flexion.

	Load (kg) at each tendon				
Experiment	ED	FDS	FDP	RIO	UIO
Full Flexion	0.36	0.079	F(t)	0.041	0.041
IPJ Flexion	0.5	0.079	F(t)	0.011	0.011

Table 5.1: Loads at each of the tendons, FDP tendon connected to slider at applies force at each time step F(t)

The kinematic validation focused on evaluating tendon displacement and moment arm during full finger flexion. These metrics are indicators of whether the model accurately represents the muscle-tendon geometry, which is important for generating realistic joint forces and movements. For the kinetic validation, the joint angles obtained from inverse kinematics were compared with those derived from forward dynamics. The flexor tendon force recorded during the experiments was also compared against the simulation results.

During the full flexion experiment, the PIP, and DIP joints were kept as stationary as possible during MCP flexion to isolate the tendon displacement contributing solely to the MCP joint. Subsequently, the PIP and DIP joints were allowed to flex. The moment arm of the tendons around the MCP joint was computed. During the IPJ flexion experiment, the MCP joint was kept as stationary as possible, and the tendon displacement of the PIP joint was used to compute the moment arm.

5.2. Data Analysis

5.2.1. Preprocessing of Experimental Data

Before analyzing the experimental data, it was necessary to preprocess the raw data to ensure smoother results, using the Motive Software:

- Marker Adjustment: For motion capture data, any misaligned or missing markers were adjusted or interpolated to maintain data integrity, which is crucial for the inverse kinematics calculations.
- Filtering and Smoothing: Raw motion capture data were filtered to remove noise. A 4th-order Butterworth filter with a cut-off frequency of 1 Hz was applied to the marker data to filter and smooth the raw measurements. The choice of a low cut-off frequency was deliberate, as it provided the smoothest data while retaining critical information. The filter effectively minimized high-frequency noise and jaggedness in the raw data without significantly affecting the signal of interest. This approach was particularly beneficial given that the raw data exhibited only small jagged errors, ensuring that the key features of the data were preserved while overall maintaining the data quality.

5.2.2. Inverse Kinematics (IK Tool)

Inverse kinematics (IK) was employed to calculate the joint angles from the motion capture data. Using OpenSim with the IK Tool, the recorded marker data from the mechanical finger was processed to calculate joint angles over time. The accuracy of the IK results was assessed by calculating error metrics such as total squared error, root mean squared error (RMSE), and maximum marker error. According to the software documentation, an acceptable accuracy is that maximum marker error should be less than 2–4 cm with a markers RMSE under 2 cm [40].

5.2.3. Tendon Excursion and Moment Arm Calculation

The moment arm of the mechanical finger was calculated using the tendon excursion method, whereby the tendon displacement data from the experiments and joint angle data from OpenSim were used. This method is only applicable to tendon excursion based on a single joint rotation. The moment arm is defined as the ratio of the rate of change of tendon excursion to the rate of change of the joint angle:

$$r(t) = \frac{\frac{dl(t)}{dt}}{\frac{d\theta(t)}{dt}} = \frac{\dot{l}(t)}{\dot{\theta}(t)}$$

where:

- $\dot{l}(t) = \frac{dl(t)}{dt}$ is the rate of change of tendon displacement with respect to time, $l(t)$, obtained from experimental data.
- $\dot{\theta}(t) = \frac{d\theta(t)}{dt}$ is the rate of change of joint angle with respect to time, $\theta(t)$, obtained from OpenSim.

The moment arms at the MCP and PIP joints were calculated based on the following approach:

- MCP Joint Moment Arm: The moment arm of the tendons at the MCP joint was determined during a trial involving MCP joint flexion. In this scenario, most of the tendon displacement was attributed to the flexion of the MCP joint. Using the experimental tendon displacement data and the joint angles derived from the IK results, the moment arm was computed as the rate of change of tendon displacement with respect to the MCP joint angle.

- PIP Joint Moment Arm: The moment arms around the PIP joint were computed during a trial that involved isolated interphalangeal joint (IPJ) flexion. The focus was on the ED and FDS tendons, as these tendons directly insert into the middle phalanx and therefore contribute significantly to PIP flexion. The moment arms were calculated similarly by using the tendon displacement data and IK-derived joint angles specific to the IPJ flexion trial.

To compute the moment arm of the mechanical finger, a second-order polynomial fit was applied to the displacement and angle data. This polynomial fit was then analytically differentiated to obtain the moment arm and reduce oscillations [41, 42]. For the OpenSim model, the tendon excursion and moment arm are derived directly from the model using joint angles obtained from the IK Tool. By varying the joint angles, the model calculates the corresponding tendon excursion and moment arm based on its defined geometry paths.

This calculation provided a dynamic assessment of the moment arm throughout the motion and was used to verify the simulation moment arm. This comparison verfies whether the simulation accurately modeled the muscle-tendon geometry and force transmission during movement.

5.2.4. Forward Dynamics (FD)

The forward dynamics (FD) simulation was run in OpenSim using tendon displacements from the experimental data as input to predict joint angles and flexor tendon force over time. The joint angles predicted by the forward dynamics simulation were compared with those obtained from the inverse kinematics analysis to verify the simulation's accuracy. Flexor tendon force calculated by the simulation was compared to the force recorded during the experiments obtained from the force sensor, focusing on validating the kinetic aspects, particularly the contribution of the Lateral Bands to the IPJ coupling mechanism.

5.2.5. Model Verification Metrics

The model's accuracy was assessed using the Mean Absolute Error (MAE) between the experimental data and the simulation results, along with its standard deviation (SD). This approach is commonly used in biomechanical and computational modeling studies to evaluate simulation accuracy. After calibrating the motion capture system, which resulted in a mean array error of 0.1 mm and a mean wand error of 0.05 mm, it's important to note that these calibration errors set the lower bound for measurement accuracy. Consequently, any MAE within these error margins represents the best possible accuracy achievable for the comparison.

Mean Absolute Error (MAE) is calculated as follows:

$$\text{MAE} = \frac{1}{n} \sum_{i=1}^{n} |y_i - \hat{y}_i|$$

where:

- n is the number of data points.
- y_i represents the observed (experimental) value.
- $\hat{y}_i$ represents the predicted (model) value.
- $|y_i - \hat{y}_i|$ is the absolute error for each data point.

5.3. Conclusion

This chapter detailed the methodology and experimentation used to verify the accuracy of the OpenSim model by comparing its performance with that of a mechanical finger. The experimental design utilized a motion capture system to record joint angles and tendon displacements during finger flexion under varying loads. The setup included marker placements on the mechanical finger and tendons and data preprocessing to ensure reliable results. A force sensor was utilized to measure the flexor tendon force, verifying the model's kinetic accuracy. Key experiments assessed the model's ability to replicate both full finger flexion and isolated IPJ flexion. Inverse kinematics and forward dynamics analyses were employed to compare experimental data with simulation results, ensuring that the model accurately reflected real-world conditions. The tendon displacement, calculated moment arms, joint angles and tendon forces were compared against experimental values, while Mean Absolute Error (MAE) metrics provided a quantitative measure of the model's accuracy.

6

Results

Verification of model estimation is essential to estimate the accuracy of the simulation results. This chapter begins with the inverse kinematics (IK) results to assess how accurately the model tracks the marker data of the mechanical finger, both visually and by the inverse kinematics marker error. Following this, tendon displacements and moment arms from the mechanical finger and the simulation model are compared, using joint angles derived from the inverse kinematics results. At last, the results from the forward dynamics (FD) simulation results are shown to evaluate the model's ability to replicate joint angles and forces, and focusing on the model's kinetics and the IPJ coupling mechanism.

6.1. Inverse Kinematics

6.1.1. Inverse Kinematics Results (IK Tool)

The mean total squared error, mean RMSE marker and maximum marker error of each trial is shown in Table 6.1.

Experiment	Trial	Mean Total squared error (mm)	Mean RMSE marker (mm)	Max marker error (mm)
Full Flexion	001	4.56e-3	0.67	3.4
	002	5.53e-3	0.74	3.3
	003	5.49e-3	0.69	2.9
IPJ Flexion	001	2.72e-3	0.51	3.0
	002	9.55e-3	0.91	2.7
	003	1.54e-3	0.39	2.1

Table 6.1: The mean total squared error, mean RMSE marker and maximum marker error of each trial

The average total squared error across all trials ranged from $1.54e-3$ mm to $9.55e-3$ mm, with an average of $4.89e-3$ mm across all markers. The marker error of each trial is close within each other with an average marker RMSE of all trials is 0.65 mm, with maximum marker error was found on the marker located at the metacarpal bone of 3.4 mm. Figures 6.1 and 6.2 shows the difference between the real position and the IK results for full finger flexion and the IPJ flexion trial, respectively.

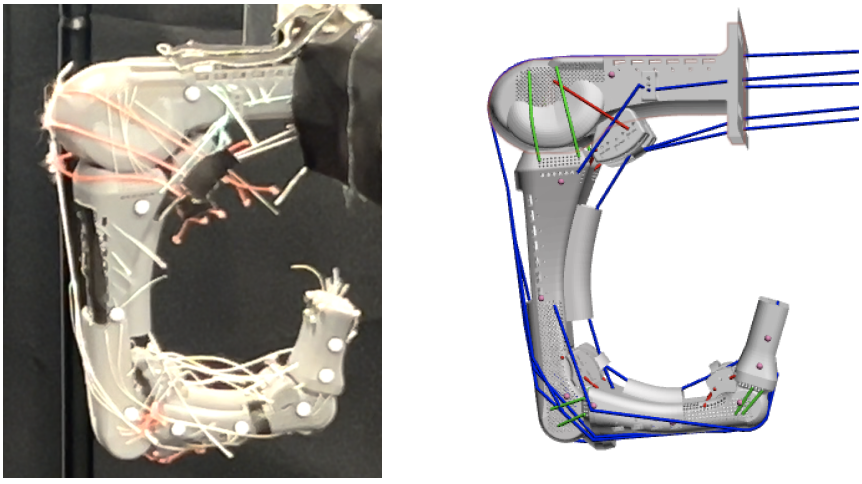

(a) Mechanical finger **(b)** IK result

Figure 6.1: End position from Full Flexion trial 003, mechanical finger vs inverse kinematics (IK) result

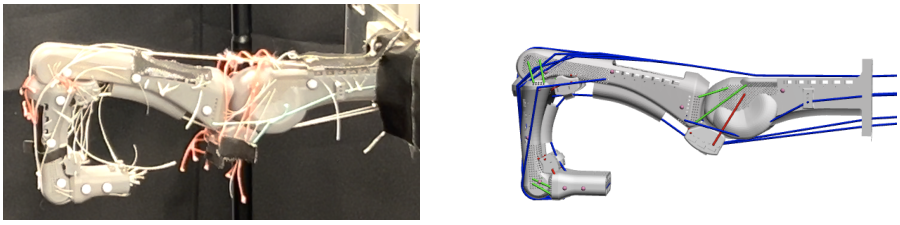

(a) Mechanical finger **(b)** IK result

Figure 6.2: End position from IPJ Flexion trial 002, mechanical finger vs inverse kinematics (IK) result

6.1.2. Tendon Excursion

The total tendon displacement of the simulation model is compared with the experimental marker data, only during the finger motion (static begin and end not included). The MAE and standard deviation across all trials was calculated for each tendon, which is given in Table 6.2.
The overall MAE for each tendon is; ED: 1.048 ± 0.63 mm, FDS: 0.493 ± 0.44 mm, FDP: 0.697 ± 0.72 mm, RIO: 0.833 ± 0.57 mm, UIO: 0.790 ± 0.51 mm. The results showed that the model's predictions were generally close to the experimental data, with an average displacement error of less than 1 mm. The comparison between the experimental data and simulation model total tendon displacement as function of the MCP and PIP joints are shown in Figure 6.3 and Figure 6.4.

	Mean absolute error displacement, milimeters (mm) (SD)					
Experiment	Trial	ED	FDS	FDP	RIO	UIO
Full Flexion	001	1.21(0.86)	0.78(0.38)	0.65(0.48)	1.04(0.43)	1.39(0.58)
	002	1.15(0.94)	0.58(0.43)	0.69(0.59)	0.81(0.52)	0.42(0.33)
	003	1.55(0.73)	1.00(0.72)	0.72(0.69)	2.03(1.10)	0.83(0.41)
IPJ Flexion	001	0.78(0.25)	0.13(0.09)	0.93(0.85)	0.31(0.31)	0.51(0.52)
	002	0.67(0.26)	0.33(0.41)	0.93(0.80)	0.49(0.39)	1.26(0.75)
	003	0.93(0.28)	0.14(0.38)	0.79(0.84)	0.32(0.20)	0.33(0.32)

Table 6.2: Mean absolute error (SD) between experimental data and simulation model of the total tendon displacement during full flexion and IPJ flexion trials

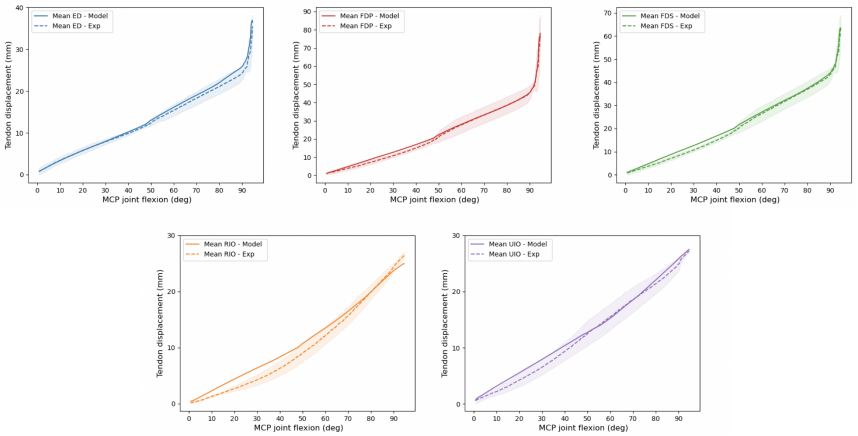

Figure 6.3: Total tendon displacement (mm) of experiment Full Flexion against MCP joint flexion angle (deg), experimental vs model, shaded areas are standard deviation of experimental data

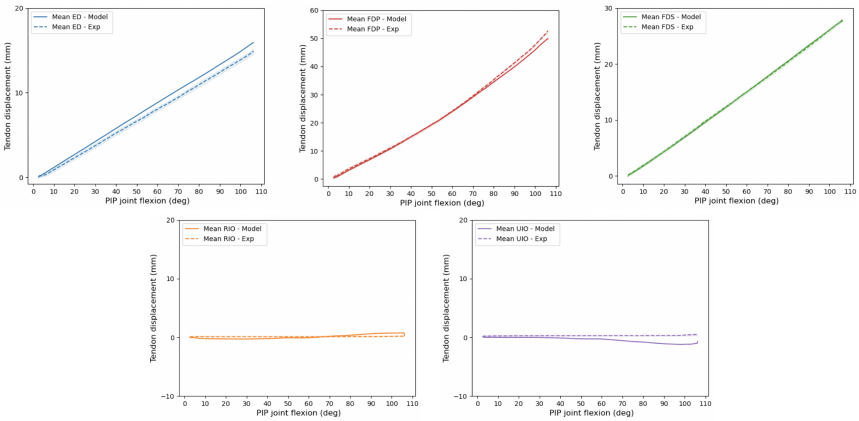

Figure 6.4: Total tendon displacement (mm) of experiment IPJ Flexion against PIP joint flexion angle (deg), experimental vs model, shaded areas are standard deviation of experimental data

6.1.3. Moment Arm

The moment arms of the tendons around the finger joints were verified against experimental measurements to assess the model's accuracy in simulating tendon-driven joint mechanics. The mean moment arm from the experimental data was compared to the OpenSim model for both the MCP joint (Figure 6.5) and the PIP joint (Figure 6.6). The plotted moment arms showed good agreement between the model's predictions and the experimental measurements, with the average MAE(SD) reported in Table 6.3. Overall, the moment arm verification results indicate that the model captures the relationship between the tendon forces and joint torques with an accuracy of ± 1.23 mm.

	Mean absolute error, milimeters (mm) (SD)				
Joint	ED	FDS	FDP	RIO	UIO
MCP_{FE}	1.10(0.78)	0.34(0.34)	1.07(0.45)	2.91(1.52)	1.83(1.38)
PIP	0.78(0.30)	0.57(0.28)	-	-	-

Table 6.3: Mean absolute error(SD) between the calculated mechanical finger moment arm and the OpenSim model moment arm

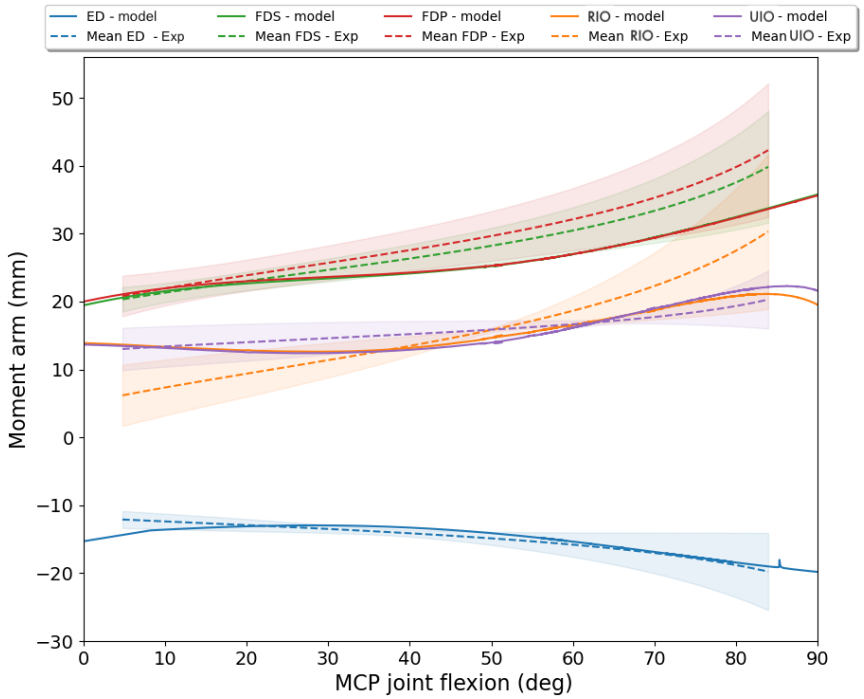

Figure 6.5: Mean Moment arms of the tendons as a function of the MCP joint during Full Flexion of calculated moment arm (Exp) vs simulation model moment arm. The shaded areas are the standard deviation of the experimental data

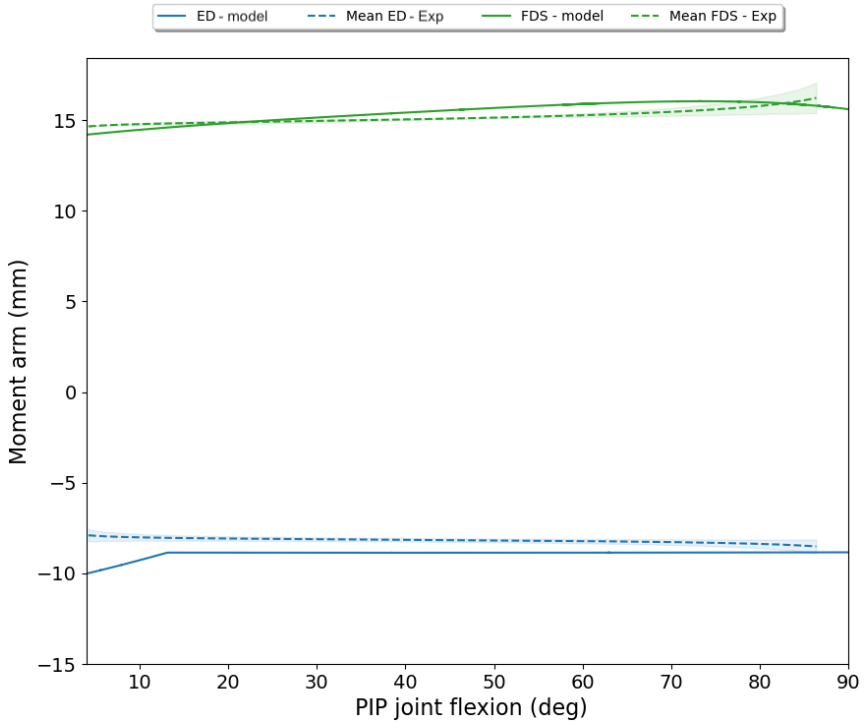

Figure 6.6: Mean Moment arms of the tendons as a function of the PIP joint during IPJ Flexion of calculated moment arm (Exp) vs simulation model moment arm. The shaded areas are the standard deviation of the experimental data

6.2. Forward Dynamics (FD)

6.2.1. Joint Angle and Tendon Force Comparison

The Mean Absolute Joint Angle Error (MAJAE) and standard deviation for each joint across all trials are presented in Table 6.4, comparing the forward dynamics simulation with the inverse kinematics (IK) analysis. The results graph comparison of each trial could be found in the Appendix C.
The average MAJAE across all trials is: MCP_{FE} 1.34 ± 0.83 deg, MCP_{AB} 1.99 ± 1.53 deg, PIP 1.68 ± 1.60 deg, and DIP 2.01 ± 1.45 deg. Similarly, the MAE for flexor tendon force comparisons between the simulation and experimental data, averaged 0.91 ± 0.83 N. The mean FDP tendon force comparison is shown in Figure 6.11 of both the Full Flexion and IPJ Flexion experiments, where a larger deviation is found at the beginning of the motion, where mostly MCP joint flexion occurs at Full Flexion.

	Mean absolute joint angle error, deg (SD)					FDP Tendon force error (SD)
Experiment	trial	MCP_{FE}	MCP_{AB}	PIP	DIP	
Full Flexion	001	1.13(0.64)	2.32(1.11)	1.05(1.06)	1.01(0.74)	0.79(0.64)
	002	1.77(0.97)	1.75(0.80)	1.90(1.84)	1.73(1.07)	1.00(0.97)
	003	1.27(1.16)	2.05(1.73)	2.61(2.30)	2.91(1.49)	0.82(1.16)
IPJ Flexion	001	0.52(0.28)	1.62(1.74)	1.82(1.69)	2.37(1.71)	1.30(0.28)
	002	2.23(1.09)	3.40(2.40)	1.19(0.91)	2.63(2.20)	0.67(1.09)
	003	1.10(0.35)	0.82(0.61)	1.52(1.31)	1.42(0.95)	0.90(0.35)

Table 6.4: Mean absolute error (SD) between joint angles of the IK results and FD results, and the FDP force between the experimental measurement and FD results

Friction Force Estimation

A contributing factor to the joint angle difference and the tension is due to the absence of friction in the model between the bones of the mechanical finger, which is not implemented in the simulation model. To assess this impact, an estimation of the friction force and friction coefficient at the MCP joint was calculated based on measurements from the Full Flexion experiments.
When the finger is in static equilibrium, the forces and torque at the MCP joint must balance to prevent movement. Each tendon exerts a force that contributes to the overall torque around the MCP joint, as there is a weight attached to each tendon (except FDP tendon). To calculate the normal force at the MCP joint, the gravitational force of the weights attached to the tendons is used, adjusted by the cosine of the joint angle θ, to account for the non-zero angle of the MCP joint. Thus, the normal force is determined as:

$$F_N = F_g * cos(\theta) \tag{6.1}$$

where F_g is the gravitation force of the weights attached at the tendons, from Table 5.1.

The finger begins to flex when a specific force is applied to the FDP tendon, where the torque produced by the FDP tendon is sufficient to overcome the static friction. This implies that the frictional force resisting motion at the MCP joint is directly related to this threshold force. The pull force on the FDP tendon, as measured by the force sensor, is the force that initiates MCP joint flexion. Therefore, the friction force can be derived from this threshold force, as it overcomes the static friction. The torque generated by the FDP tendon is:

$$T_f = F_{FDP} \cdot r_{FDP} \tag{6.2}$$

where r_{FDP} is the moment arm of the FDP tendon at the MCP joint. The frictional force is connected to the frictional torque through the following relationship:

$$T_f = F_f \cdot r_{MCPjoint} \tag{6.3}$$

where $r_{MCPjoint}$ is the average joint center of the MCP joint (from Table 3.2). Finally, the friction coefficient μ is calculated as the ratio of the friction force to the normal force:

$$\mu = \frac{F_N}{F_f} \tag{6.4}$$

Following these calculation steps, the estimated friction force and coefficient at the MCP joint is found to be 2.34 N and 0.460 respectively.

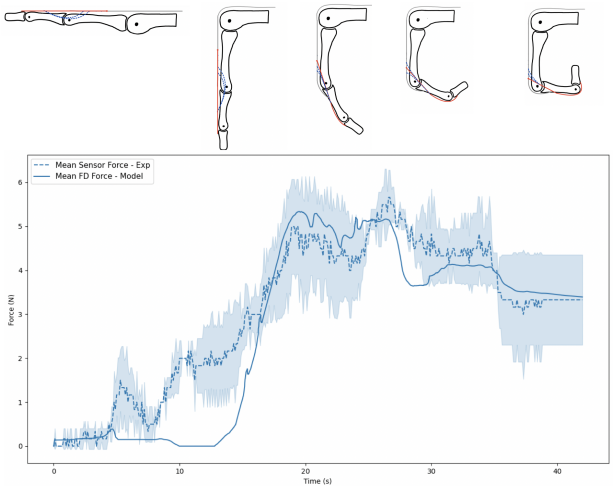

(a) Mean FDP tendon force [N] comparison experimental results vs FD results of simulation model, from Full Flexion experiment. The shaded areas are the standard deviation of the experimental data

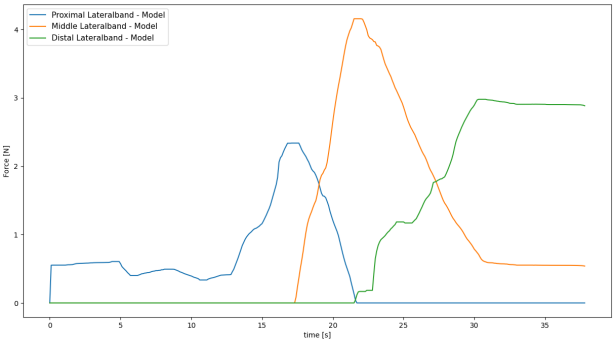

(b) Tension [N] in Lateral Bands of FD simulation model, of Trial 001 Full Flexion

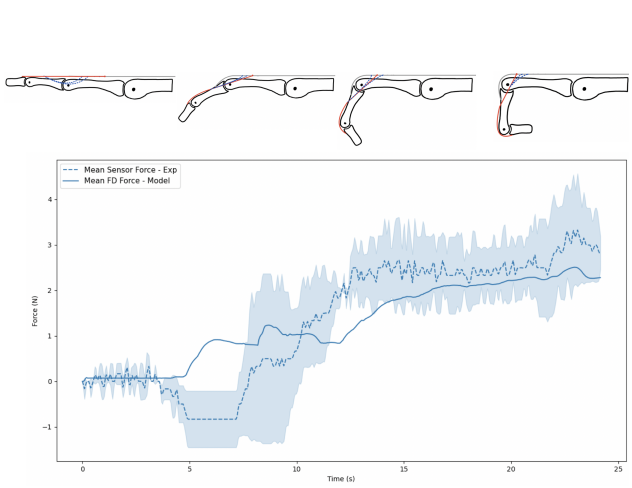

(c) Mean FDP tendon force [N] comparison experimental results vs FD results of simulation model, from IPJ Flexion experiment. The shaded areas are the standard deviation of the experimental data

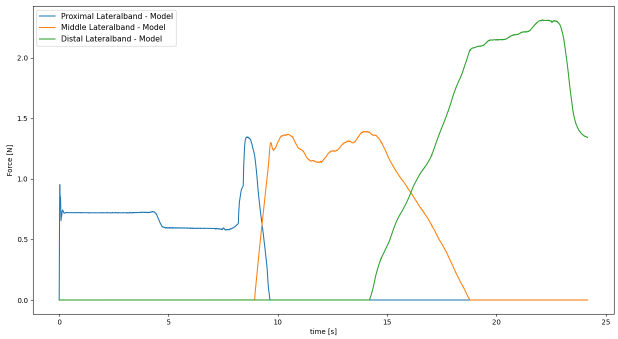

(d) Tension [N] in Lateral Bands of FD simulation model, of Trial 003 IPJ Flexion

Figure 6.11: Mean FDP tendon force [N] comparison experimental results vs Forward Dynamics (FD) results of simulation model with the lateralband tension from the FD simulation given from IP and Full Flexion trials

6.2.2. The Lateral Band's Role in IPJ coupling

The mean PIP and DIP joint results across all trials from both the IK and FD simulation are presented in Figure 6.12. This graphs shows the coupled relation between these joints (IPJ coupling), with the FD simulation results mostly falling within the standard deviation of the IK simulation results. The simulation achieved a MAE of 0.84 degrees and a standard deviation of 0.56 degrees and error ranging from 0.0015 to 2.05 degrees.

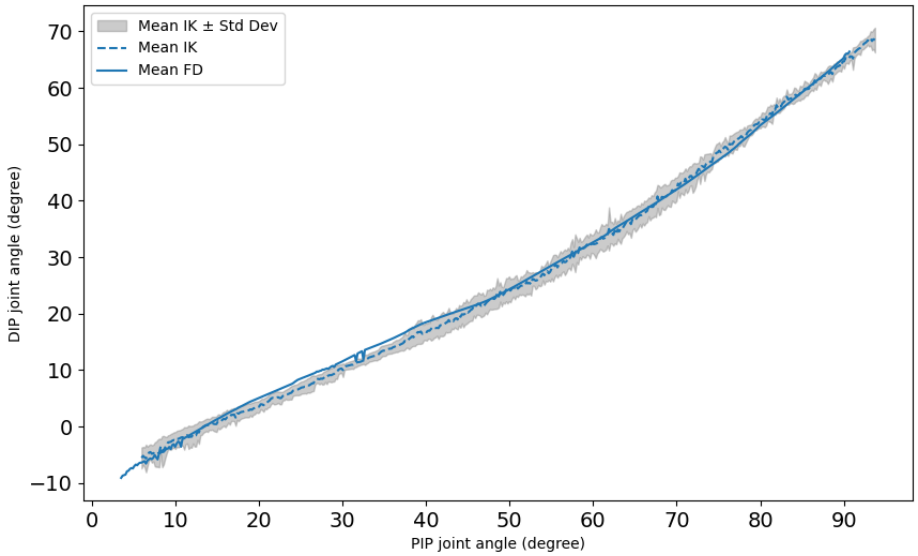

Figure 6.12: IPJ coupling analysis as the coupled relation between the PIP and DIP joints during IPJ flexion. The comparison between the mean values of the six trials of the IK and FD simulation results

In addition to capturing joint angles, the simulation results demonstrated that the force in the Lateral Band was transferred from the proximal to the distal Lateral Bands, as shown in Figure 6.11. It should also be noted that the high peak clearly seen in the forces of the Lateral Bands are caused by slipping of the ED tendon and Lateral Bands from the wrapping surface at the MCP joint. Figure 6.13 further highlights the importance of incorporating the Lateral Bands for accurate IPJ coupling. Without the Lateral Bands, excessive flexion occurs in the DIP joint.

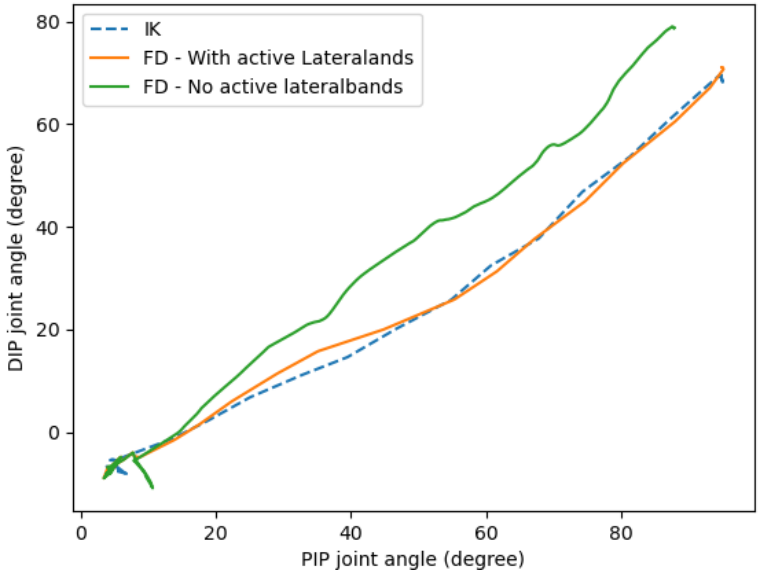

Figure 6.13: Comparison of IPJ coupling between the IK simulation vs FD simulation with active and inactive Lateral Bands, Trial 001 Full Flexion

7

Discussion and Recommendations

The aim of this study is to better understand the function and interaction of Lateral Bands in coordinate finger flexion with the developed musculoskeletal model. This chapter will first evaluate the simulation model results against experimental data from the mechanical finger to determine its accuracy by verification. The focus will be on joint accuracy, tendon displacement, and moment arms to ensure realistic representation of joint kinematics and muscle-tendon geometry. Where applicable, the results are compared with relevant published research. Following this verification, the role of Lateral Bands in finger flexion, joint coupling, and force distribution will be examined. The limitations of the model are addressed, and finally recommendations for future improvements.

7.1. Inverse Kinematics Analysis

7.1.1. IK Joint Angles

Based on the IK results, the joint angles are within the acceptable range for marker data tracking with an average total squared error across all trials ranged from $1.54e-3$ mm to $9.55e-3$ mm, and an average of $4.89e-3$ mm across all markers. These results demonstrate that the model tracks the experimental data with a high degree of accuracy, indicating that the kinematic structure of the model closely aligns with the actual mechanics of the finger. Some discrepancies were observed during MCP joint flexion. The maximum marker error of 3.4 mm was recorded at the metacarpal bone during the Full Flexion experiment in Trial 001, specifically at a MCP joint angle of 40 degrees. In contrast, similar errors were not observed in the other two trials, where the errors occurred at a MCP joint angle of 80 degrees. Examination of the experimental data revealed slight drifting of the metacarpal marker, but the extent of this drift was minimal and likely not the cause of the larger errors. The inconsistencies across trials suggest a potential misalignment between the joint center of rotation in the simulation model and the mechanical finger. Although, the marker errors exceed the calibration error range of 0.05 to 0.1 mm, they are confined to a specific range of motion. These discrepancies could potentially be addressed by adjusting the joint center or ellipsoid joint size and marker placement in the model.
Moreover, visual inspection shows that the model effectively reproduces the movement patterns observed in the experimental data. The average marker RMSE of 0.65 mm indicate that the model can track the marker data, with only minor deviations. These deviations are significant lower than what is acceptable according to OpenSim documentation, considering that the model is based on a mechanical finger, which eliminates artifacts introduced by skin movement — a factor present in cadaveric studies or human subjects. This indicates that the model's joint kinematics can be used for further dynamic analysis and research.

7.1.2. Total tendon displacement

From the experimental trials compared to the simulation model, it has been gathered that the average tendon displacement error is less than 1 mm, for the overall finger motion and geometric path within the simulation model. However, slight deviations were observed in the ED tendon due to the simulation model in OpenSim not fully capturing the tautness of the Lateral Bands. In the model, the bands are not directly attached and do not share forces with the ED tendon. Consequently, a small deviation arises when IPJ flexion begins, as seen in Figure 6.3, where IPJ coupling occurs at around 50 degrees of MCP joint flexion, and Figure 6.4, which focuses solely on IPJ flexion, since the contribution of the Lateral Bands is neglected. The highest MAE was observed in the RIO tendon during trial 003, where there was increased MCP joint

adduction. In the OpenSim model, the RIO tendon is fixed and does not wrap around the MCP joint during abduction and adduction. This limitation means that the model does not account for tendon excursion during these joint movements. As a result, larger deviations are particularly notable at higher values of abduction and adduction, leading to more pronounced discrepancies in the RIO tendon measurements.
When comparing these results to those from other models that have compared simulation data with experimental data from cadaveric studies, the deviations observed here are relatively minor. Although this comparison is based on visual assessments of graph results rather than quantitative metrics, the mechanical finger simulation model shows a more precise alignment with experimental data, particularly when contrasted with the larger discrepancies observed in simulation models compared to cadaveric studies [16, 43].

7.1.3. Moment Arm

The result graphs, Figure 6.5 and 6.6 for the MCP and PIP joint respectively, show a close similarity between the moment arms computed directly from the OpenSim model and those calculated using the tendon excursion method, verifying that the model effectively simulates tendon-driven joint mechanics close to those of the mechanical finger. The moment arm verification results demonstrate that the model accurately captures the relationship between tendon forces and joint torques, with an average error of 1.23 mm. These small errors are within close range when compared to other studies, including one comparing its data to cadaveric findings [44], and another using optimization to refine muscle attachment and moment arm measurements from cadavers [45]. This verification confirms the model's functionality for simulating tendon-driven joint mechanics.

It should be noted that a limitation of the tendon excursion method is that it is only applicable when a single joint rotates in isolation with the tendon excursion, and not when multiple joints are rotating simultaneously. As a result, the observed discrepancies are primarily attributed to errors in the calculated moment arm, rather than inaccuracies in the OpenSim model's moment arm. It can be seen from the discrepancies in the moment arm primarily occur across the MCP joint in the mid-range of motion. This is due to slight flexion of the PIP and DIP joints during MCP flexion, which also contributes to tendon displacement, introducing errors in the experimental moment arm calculations. Similarly, at the start of the PIP joint flexion, higher deviations are likely occurred because the MCP joint had not yet completed its full flexion, leading to tendon excursion influenced by both MCP and PIP joint movements rather than being isolated to the PIP joint. Further insights are provided by measurements from the CAD model (refer to Table 3.2), which indicate that the ED tendon must lie flat on the joint during flexion. Based on the bone geometry, the maximum moment arm is approximately 14.5 mm for the MCP joint and around 8.2 mm for the PIP joint, closely matching the simulation results.

Deviations in the calculated moment arm for the IO tendon are caused by the MCP abduction, which could influence the accuracy of the moment arm calculation. Similarly, the variations seen in the FDS and FDP tendons stem from differences in how these tendons interact with the pulleys. In the mechanical model, these tendons shift from the top to the bottom of the pulley during flexion. The simulation model uses fixed via points for the tendons, meaning their relative positions to the pulleys remain unchanged, which could cause the observed discrepancies in moment arm calculations. The errors observed in the FDP and FDS tendons may result from changes in the mechanical finger's moment arm due to the location of the volar plates, which act as pulleys and alter the tendon path during flexion. In Appendix A this is shown for the MCP joint.

7.2. Forward Dynamics Analysis

7.2.1. FD Joint angles

The Mean Absolute Joint Angle Error (MAJAE) values indicate an alignment between the IK and FD simulation results. This indicates that the model effectively replicates the mechanical finger's movements and forces, with the incorporated anatomical joints successfully constraining the joint range of motion. The highest MAJAE was observed in the DIP joint angle, particularly in trial 003 of the Full Flexion. In this trial, it was noted that during the experiment, the ED tendon slipped off the MCP joint, which affected the tendon displacement (input to FD simulation). This, in turn, altered the forces applied to the Lateral Bands, ultimately influencing the DIP joint angle.
When compared to another study on a robotic finger simulation model, which reported MAJAE values

of 5.6 deg, 2.2 deg, 3.9 deg, and 5 deg for the MCP_{FE}, MCP_{AB}, PIP, and DIP joints respectively. The current results show a similar pattern of alignment and improvements, where the model's performance is consistent with those steady-state simulations despite being evaluated over dynamic movement [28].

7.2.2. Flexor Tendon Force

In most trials, the simulated FDP tendon force follows a curve trend similar to that of the experimental force sensor data. The low MAE values for FDP tendon forces indicate that the forward dynamics simulation accurately replicates the finger's mechanical behavior as observed experimentally. However, the tendon force error, shown in Figure 6.11, is attributable to the OpenSim model not accounting for the passive tension exerted by the weight, as there is a significant deviation at the beginning of the force curve. In the FD simulation, tendon displacement is applied as input, which corresponds to the displacement of the weights. During the forward dynamics simulation, if the weights remain stationary, they effectively do not contribute any gravitational force, since their displacement drives the simulation rather than actual physical forces. As a result, the tension is only reflected once IPJ flexion begins as the Lateral Band applies force. Comparing these results with the 3D inverse dynamic model developed by Sancho-Bru et al. (2001), which reported a maximum FDP tendon force of less than 2 N during free flexion–extension motion of the finger, reveals that the forces observed in this study are higher [10]. This discrepancy highlights the impact of friction in the mechanical finger setup.

During the experiment, the finger stayed extended with a small force applied on the FDP tendon and only began to flex slowly as the force increased, while the simulation model flexed immediately with minimal force. This discrepancy suggests that friction in the mechanical components is preventing movement. At the MCP joint, the estimated friction force is 2.34 N, with a coefficient of 0.460, indicating that friction, along with ligaments and tendons, helps keep the finger stationary. A study on 3D-printed PLA parts found friction coefficients between 0.127 and 0.354, making the friction in this setup relatively high [23]. Additionally, the force sensor, placed at the end of the FDP tendon, does not account for resistance from the pulley system or testbed, affecting the results. To obtain more accurate measurements, the sensor should be positioned between the pulley and the finger in future experiments.

7.2.3. IPJ Coupling

The IPJ coupling analysis shows that the results for the IK and FD simulations are closely aligned. This suggests that the slack length of the Lateral Bands, which depends on their length and position, has been correctly estimated. The IPJ coupling is effectively created by the correct tension developing in the Lateral Bands, where tension is transferred from one band to another. The flexor tendons begin to experience tension once the Lateral Bands start to tighten, initiating the IPJ coupling (Figure 6.11). This indicates that the Lateral Bands contribute to the tension in the FDP tendon, which is the primary contributor to DIP joint flexion. The Lateral Bands prevent the DIP joint from rotating until the PIP joint starts to rotate and slack forms in the Lateral Bands. This phenomenon is evident in the analysis, confirming the functional role of the Lateral Bands, as demonstrated in Figure 6.13. The graph illustrates the impact of inactive Lateral Bands during finger joint flexion, highlighting their importance in joint mechanics. Without active Lateral Bands, there is no constraint on DIP joint flexion, meaning the motion deviates from what is observed in the mechanical finger, thus failing to produce the expected movement pattern.

These findings align with the 2D kinematic model developed by Leijnse and Spoor (2012), on which the IPJ coupling in this model is based on. The 2D kinematic model aimed to determine the attachment point and location of the Lateral Band by matching it to experimental IPJ trajectories. Their results reported a maximum IPJ trajectory error of less than 3 degrees in 50% of cases, with the remaining cases showing errors between 3 and 12 degrees [13]. In comparison, this simulation achieved a mean absolute error (MAE) of 0.84 degrees with a standard deviation of 0.56 degrees and error ranging from 0.0015 to 2.05 degrees. These results suggest that the joint coupling mechanics in the current model are well-represented, improving its fidelity in simulating the complex biomechanics of the finger.

7.3. Model Simplification

7.3.1. Wrapping Surfaces

The forward dynamics (FD) simulation demands significant computational effort, often leading to stalls at certain positions. This issue was particularly pronounced with the wrapping surfaces. Initially, the simulation

model included torus wrapping surfaces, designed to constrain a tendon or ligament path within the inner diameter of the torus. These were intended to function as the transverse retinacular ligament, keeping the Lateral Bands radial or ulnar to the PIP joint during extension and flexion. This setup contributed to creating slack, particularly in the proximal Lateral Band, by reducing its moment arm across the PIP joint. The wrapping effect pulled the proximal Lateral Band downward, generating slack and influencing its mechanics. However, these surfaces were removed as they caused prolonged computational time, though the exact additional time could not be determined as it is not a focus of the study. Fixed points were used instead, which proved sufficient for the study and were not further investigated.
Additionally, these wrapping surfaces were added to the pulleys to mimic the behavior of the flexor tendons moving from being flush against the top pulley to a lower position during flexion. However, the inclusion of these surfaces resulted in significantly longer simulation run times, and ultimately, they were deemed unnecessary as the model can perform without them. It is also important to note that the direction in which the wrapping surfaces were allowed to rotate had to be specifically defined. Without this specification, the surfaces could wrap incorrectly in some cases, particularly during near full flexion or hyperextension.

7.3.2. Lateral Bands

This simplification was chosen to make it more manageable to adjust the length and position of the bands, reducing the need for extensive trial and error. Fewer bands allowed for more straightforward fine-tuning of their placement and function, while also decreasing the computational time. Using more bands would have increased the complexity of ensuring each band performed as intended, requiring additional testing and computational resources. By reducing the number of bands, the model maintained essential mechanical behavior with more efficient adjustments and faster computation. As noted by MacFarland et al. (2022), introducing fewer muscle actuators is recommended, as additional actuators increase the number of constraints required for force sharing in the model. Although the physical finger has five bands, the simulation can capture the key biomechanical functions with fewer bands, each representing the collective contribution of multiple physical bands. The results showed that three Lateral Bands were sufficient to replicate the IPJ coupling effect accurately, ensuring that the model produced realistic outcomes without compromising accuracy.

In the mechanical finger, five bands distribute forces more evenly during flexion, preventing excessive force on any single band. In contrast, the simulation's reduced number of bands may lead to higher cumulative forces in the FDP tendon, contributing to the observed increase in force compared to the physical setup. Additionally, since the Lateral Bands in the simulation follow the same path as the ED tendon but do not originate from it, force transmission is less dispersed.

Despite this, the higher loads in the simulation remained within the FDP's maximum capacity, and the Lateral Band forces were within acceptable limits. As no specific data exist on Lateral Band forces during dynamic simulations, the model's performance aligns with current expectations.

7.4. Recommendations

Friction and Damping Although joint friction in real human fingers is minimal, the mechanical finger experienced friction forces between the 3D-printed parts, in particular static friction. To improve the accuracy of the simulation model and better align it with the mechanical finger's behavior, it would be useful to assess the friction coefficient between the parts. This would help determine whether friction significantly impacts the overall kinematics and force, or if other factors are contributing to the differences observed.

Lateral Band Optimization The slack length is currently determined through a trial-and-error process, where adjustments are made by observing the dynamic simulation and modifying the length accordingly. This approach could be improved by using optimization techniques to identify the optimal length and positioning, depending on the initial finger position, thereby enhancing the effectiveness of the IP coupling mechanism.

Motion Capture The marker error at the MCP joint could be reduced by adding more markers either directly on the metacarpal with sticker (flat) markers or on the stationary frame. This would improve the accuracy of joint angle measurements. Additionally, improvement in the marker placement would enable a more detailed analysis of MCP abduction-adduction and axial rotation. While these aspects could be

examined with the current simulation model, they were not explored in this thesis.

Actuation of Tendons Currently, actuation is achieved using a pulley lever system, with tendon forces applied through a testbed equipped with an existing force sensor. However, incorporating stepper motors and/or potentiometers could enhance the system by directly actuating the tendons. This approach would allow precise control over tendon displacement and force, providing comprehensive data on the dynamic behavior of the mechanical finger, effectively transforming it into a more robotic-like finger. Such detailed information could be used to refine the simulation model or for further verification purposes.

Model Validation Finally, by incorporating cadaveric parameters, such as muscle-tendon anatomical properties, the model can be adjusted and validated against cadaveric studies, thereby enhancing its fidelity to real-world conditions. Once this validation proves to be successful, the simulation model will be completely validated, making it a more reliable tool for clinical applications such as surgical treatment, tendon reconstruction, and the study of finger pathologies.

8

Conclusion

This study aimed to improve computational musculoskeletal models for better understanding the function of Lateral Bands and their role in coordinated finger flexion. A successful musculoskeletal model was developed in OpenSim that replicates the anatomical joints and Lateral Band structures of an anthropomorphic mechanical finger. By basing the model on the mechanical finger, it benefits from simplifications that reduce complexity and improve verification reliability.

Firstly, the model incorporated anatomical joints that closely match the bone geometry and joint articulation of the mechanical finger, allowing for more realistic joint rotation that mirrors natural joint curvature. Adding joint ligaments enabled joint constraints, with ligaments adjusting from slack to taut based on joint position. Verification of joint kinematics showed that the model's kinematic structure aligns closely with the actual mechanics of the finger. Secondly, muscle-tendon geometry was verified, assessing tendon displacement and moment arms to determine how well the model represents muscle-tendon geometry and joint torque contributions. Results indicated that the model effectively simulates tendon-driven joint mechanics similar to those of the mechanical finger. Lastly, by applying external forces to the flexor digitorum profundus (FDP) tendon, the model demonstrated how forces are transferred and distributed among the Lateral Bands. This reflected the dynamic slack and taut behavior observed in the mechanical finger, offering valuable insights into the Lateral Bands' role in finger mechanics and providing a quantitative understanding of their function. The significant advancement of this model lies in its ability to offer deeper insights into force distribution within the Lateral Bands and their important role in finger flexion.

Future research could build on this model to further investigate the role of Lateral Bands in force distribution and their interaction with joint mechanics. For instance, exploring how activating other tendons, such as the flexor digitorum superficialis (FDS), affects interphalangeal joint (IPJ) coupling and finger coordination could provide new insights. The model could be adapted to examine the effects of adding or removing Lateral Bands on finger coordination, not only during flexion but also extension. Given that force distribution is crucial for finger health and can influence injury and deformity, adapting the model to replicate and study these conditions could lead to new solutions and a better understanding of finger dynamics. This research could ultimately serve as a valuable tool for clinical applications, aiding in the prevention and treatment of finger-related injuries and disorders.

References

[1] Susan M. Craig. “Anatomy of the joints of the fingers”. In: *Hand Clinics* 8.4 (Nov. 1992), pp. 693–700. DOI: 10.1016/s0749-0712(21)00736-8.

[2] Marc Garcia□Elias et al. “Extensor mechanism of the fingers. II. Tensile properties of components”. In: *The Journal of Hand Surgery* 16.6 (Nov. 1991), pp. 1136–1140. DOI: 10.1016/s0363-5023(10)80080-2.

[3] Alexander Synek et al. “Musculoskeletal models of a human and bonobo finger: parameter identification and comparison to in vitro experiments”. In: *PeerJ* 7 (Aug. 2019), e7470. DOI: 10.7717/peerj.7470.

[4] Katherine R.S. Holzbaur et al. “A model of the upper extremity for simulating musculoskeletal surgery and analyzing neuromuscular control”. In: *Annals of Biomedical Engineering* 33.6 (2005), pp. 829–840. DOI: 10.1007/s10439-005-3320-7.

[5] Kim Seng Fok et al. “Development of a finger biomechanical model and its considerations”. In: *Journal of Biomechanics* 43.4 (2010), pp. 701–713. DOI: 10.1016/j.jbiomech.2009.10.020.

[6] Daniel C. McFarland et al. “A Musculoskeletal Model of the Hand and Wrist Capable of Simulating Functional Tasks”. In: *IEEE Transactions on Biomedical Engineering* (2022). DOI: 10.1109/TBME.2022.3217722.

[7] Alexander J. Barry et al. “Development of a dynamic index finger and thumb model to study impairment”. In: *Journal of Biomechanics* 77 (Aug. 2018), pp. 206–210. DOI: 10.1016/j.jbiomech.2018.06.017.

[8] Benjamin I. Binder-Markey et al. “Incorporating the length-dependent passive-force generating muscle properties of the extrinsic finger muscles into a wrist and finger biomechanical musculoskeletal model”. In: *Journal of Biomechanics* 61 (2017), pp. 250–257. DOI: 10.1016/j.jbiomech.2017.06.026.

[9] John Z. Wu et al. “Analysis of musculoskeletal loading in an index finger during tapping”. In: *Journal of Biomechanics* 41.3 (2008), pp. 668–676. DOI: 10.1016/j.jbiomech.2007.09.025.

[10] J. L. Sancho-Bru et al. “A 3-D dynamic model of human finger for studying free movements”. In: *Journal of Biomechanics* 34.11 (2001), pp. 1491–1500. DOI: 10.1016/S0021-9290(01)00106-3.

[11] Joaquín L. Sancho-Bru et al. “A 3D biomechanical model of the hand for power grip”. In: *Journal of Biomechanical Engineering* 125.1 (2003), pp. 78–83. DOI: 10.1115/1.1532791.

[12] Mojtaba Mirakhorlo et al. “A musculoskeletal model of the hand and wrist: model definition and evaluation”. In: *Computer Methods in Biomechanics and Biomedical Engineering* 21.9 (July 2018), pp. 548–557. DOI: 10.1080/10255842.2018.1490952.

[13] J. N.A.L. Leijnse et al. “Reverse engineering finger extensor apparatus morphology from measured coupled interphalangeal joint angle trajectories - a generic 2D kinematic model”. In: *Journal of Biomechanics* 45.3 (2012), pp. 569–578. DOI: 10.1016/j.jbiomech.2011.11.002.

[14] N. Brook et al. “A biomechanical model of index finger dynamics”. In: *Medical Engineering and Physics* 17.1 (1995), pp. 54–63. DOI: 10.1016/1350-4533(95)90378-0.

[15] Alexander MacIntosh et al. “An open-source model and solution method to predict co-contraction in the finger”. In: *Computer Methods in Biomechanics and Biomedical Engineering* 20.13 (Aug. 2017), pp. 1373–1381. DOI: 10.1080/10255842.2017.1364732.

[16] Mojtaba Mirakhorlo et al. “Anatomical parameters for musculoskeletal modeling of the hand and wrist”. In: *International Biomechanics* 3.1 (2016), pp. 40–49. DOI: 10.1080/23335432.2016.1191373.

[17] Dan Qiu et al. “Orthopaedic applications of a validated force-based biomechanical model of the index finger”. In: *Physiology & behavio* (Aug. 2017). DOI: 10.1109/embc.2014.6944504.

[18] Alexander Synek et al. “The effect of the extensor mechanism on maximum isometric fingertip forces: A numerical study on the index finger”. In: *Journal of Biomechanics* 49.14 (Oct. 2016), pp. 3423–3429. DOI: 10.1016/j.jbiomech.2016.09.004.

[19] Francisco J. Valero-Cuevas et al. “Large index-fingertip forces are produced by subject-independent patterns of muscle excitation”. In: *Journal of Biomechanics* 31.8 (1998), pp. 693–703. DOI: 10.1016/S0021-9290(98)00082-7.

[20] Anton Dogadov et al. “The Detailed Model of the Middle Finger Extensor Mechanism for Understanding the Role of Intercrossing Fibers”. In: (2022). DOI: hal-03955597.

[21] James. A. Tigue et al. “Simulating Tendon Shortening During Flexor Tendon Repair Surgery Using A Biomechanical Model and Robotic Testbed”. In: *Proceedings of the IEEE RAS and EMBS International Conference on Biomedical Robotics and Biomechatronics* (Nov. 2020). DOI: 10.1109/biorob49111.2020.9224447.

[22] James. A. Tigue et al. “Validation of Fingertip Force and Finger Pose in the UART Finger and Bond Graph Tendon Model During Surface Contact”. In: Tysons, Virginia, USA, Oct. 2017.

[23] van Youri Delft. *Design and Analysis on the friction characteristic of a 3D printed mechanical Synovial Joint Exploring the parameters of a novel 1-DoF synovial finger design*. Master’s thesis. Available at https://repository.tudelft.nl/record/uuid:7f6f7295-927b-4fc8-86a9-c7596bcbd176. 2023.

[24] Jacob Van Ooijen. *Humanising robot fingers: Design, prototyping, and validation of an anthropomorphic robot finger with humanoid joint-ligament systems, tendon configurations and supporting ligaments*. Master’s thesis. Available at https://repository.tudelft.nl/record/uuid:4b693437-e31c-4ef3-bc10-781cfd5b34d8. 2022.

[25] Taylor D. Niehues et al. “Development and validation of modeling framework for interconnected tendon networks in robotic and human fingers”. In: *Proceedings - IEEE International Conference on Robotics and Automation* (May 2017). DOI: 10.1109/icra.2017.7989481.

[26] A. D. Deshpande et al. “Mechanisms of the anatomically correct testbed hand”. In: *IEEE/ASME Transactions on Mechatronics* 18.1 (Feb. 2013), pp. 238–250. DOI: 10.1109/tmech.2011.2166801.

[27] D.D. Wilkinson et al. “An extensor mechanism for an anatomical robotic hand”. In: *Proceedings - IEEE International Conference on Robotics and Automation* (Mar. 2004). DOI: 10.1109/robot.2003.1241602.

[28] James A. Tigue et al. “Calibration and Validation of Dynamic Model for Simulating Robotic Finger Kinematics and Contact Forces”. In: *ASME 2019 Dynamic Systems and Control Conference, DSCC 2019* (Nov. 2019). DOI: 10.1115/dscc2019-8961.

[29] Beatriz León et al. *From robot to human grasping simulation*. Vol. 19. 2014. DOI: 10.1007/978-3-319-01833-1.

[30] E Okwumabua et al. *Anatomy, Shoulder and Upper Limb, Hand Muscles*. 2022. URL: https://www-ncbi-nlm-nih-gov.tudelft.idm.oclc.org/books/NBK537229/.

[31] Lynn Lippert. *Clinical kinesiology and anatomy*. 4th ed. Jan. 2006.

[32] Dan Hu et al. “Biomechanical Analysis of the Human Finger Extensor Mechanism during Isometric Pressing”. In: *PLOS ONE* 9.4 (Apr. 2014), e94533. DOI: 10.1371/journal.pone.0094533.

[33] M Taqi et al. *Finger Dislocation*. 2022. URL: https://www-ncbi-nlm-nih-gov.tudelft.idm.oclc.org/books/NBK551508/.

[34] Joshua M. Adkinson et al. “The clinical implications of the oblique retinacular ligament”. In: *The Journal of Hand Surgery* 39.3 (Mar. 2014), pp. 535–541. DOI: 10.1016/j.jhsa.2013.12.011.

[35] Christoph Lutter et al. “Dynamic study of the finger interphalangeal joint volar plate—motion analysis with magnetic resonance cinematography and histologic comparison”. In: *Skeletal Radiology* 52.8 (Feb. 2023), pp. 1493–1501. DOI: 10.1007/s00256-023-04288-6.

[36] J.N.A.L. Leijnse et al. “Kinematic evaluation of the finger’s interphalangeal joints coupling mechanism—variability, flexion–extension differences, triggers, locking swanneck deformities, anthropometric correlations”. In: *Journal of Biomechanics* 43.12 (Aug. 2010), pp. 2381–2393. DOI: 10.1016/j.jbiomech.2010.04.021.

[37] Adam Kewley et al. “OpenSim Creator”. In: *Zenodo* (2024). DOI: 10.5281/zenodo.7575937.

[38] Ajay Seth et al. “Minimal formulation of joint motion for biomechanisms”. In: *Nonlinear Dynamics* 62.1-2 (May 2010), pp. 291–303. DOI: 10.1007/s11071-010-9717-3.

[39] *API: OpenSiM::EllipsoidJoint Class Reference*. URL: https://simtk.org/api_docs/opensim/api_docs/classOpenSim_1_1EllipsoidJoint.html.

[40] *Getting Started with Inverse Kinematics - OpenSim Documentation - OpenSim*. URL: https://opensimconfluence.atlassian.net/wiki/spaces/OpenSim/pages/53090032/Getting+Started+with+Inverse+Kinematics.

[41] Ruoli Wang et al. “Passive mechanical properties of human medial gastrocnemius and soleus musculotendinous unit”. In: *BioMed Research International* 2021 (Feb. 2021), pp. 1–12. DOI: 10.1155/2021/8899699.

[42] Florian Fath et al. “Direct comparison of in vivo Achilles tendon moment arms obtained from ultrasound and MR scans”. In: *Journal of Applied Physiology* 109.6 (Dec. 2010), pp. 1644–1652. DOI: 10.1152/japplphysiol.00656.2010.

[43] John Z. Wu et al. “A practical biomechanical model of the index finger simulating the kinematics of the muscle/tendon excursions”. In: *Bio-Medical Materials and Engineering* 20.2 (2010), pp. 89–97. DOI: 10.3233/BME-2010-0618.

[44] Lucas Engelhardt et al. “A new musculoskeletal AnyBody,Ñ¢ detailed hand model”. In: *Computer Methods in Biomechanics and Biomedical Engineering* 24.7 (2020), pp. 777–787. DOI: 10.1080/10255842.2020.1851367.

[45] Jong Hwa Lee et al. “Finger muscle attachments for an OpenSim Upper-Extremity model”. In: *PLoS ONE* 10.4 (Apr. 2015), e0121712. DOI: 10.1371/journal.pone.0121712. URL: https://doi.org/10.1371/journal.pone.0121712.

A

Anthropomorphic Mechanical Finger Closeup

A.1. Lateral Bands

(a) In finger extension, the proximal Lateral Bands are located near the MCP joint and remain taut.

(b) During mid IPJ flexion, the extensor tendon moves distally, shifting the Lateral Bands with it. The proximal Lateral Bands become slack, while the middle Lateral Bands are taut, positioned middle of the proximal phalanx.

(c) In near full IPJ flexion, the distal Lateral Bands are taut, while the extensor tendon moves slightly less distally. The Lateral Band positions remain mostly unchanged compared to mid flexion.

Figure A.1: During IPJ flexion, the extensor tendon moves distally, creating alternating tension and slack in the Lateral Bands as force transfers from the tendon. Different Lateral Bands contribute to varying tension levels throughout the IPJ flexion.

A.2. Pulleys

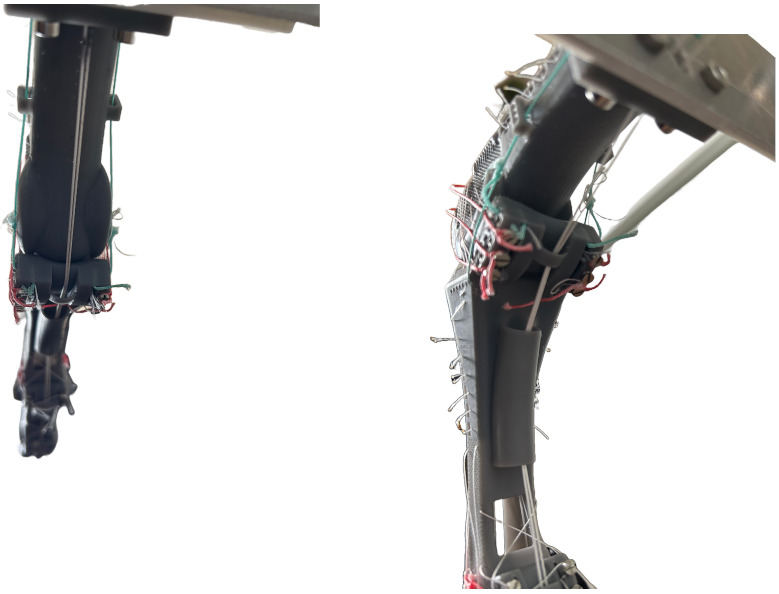

(a) In finger extension, the flexor tendons lie flush against the metacarpal and volar plate.

(b) During MCP joint flexion, the flexor tendons shift toward the pulley, moving away from their position against the volar plate.

Figure A.2: Bottom view: Flexor tendons change locations at the pulleys, separates from the top surface of the volar plate and metacarpal, increases moment arm

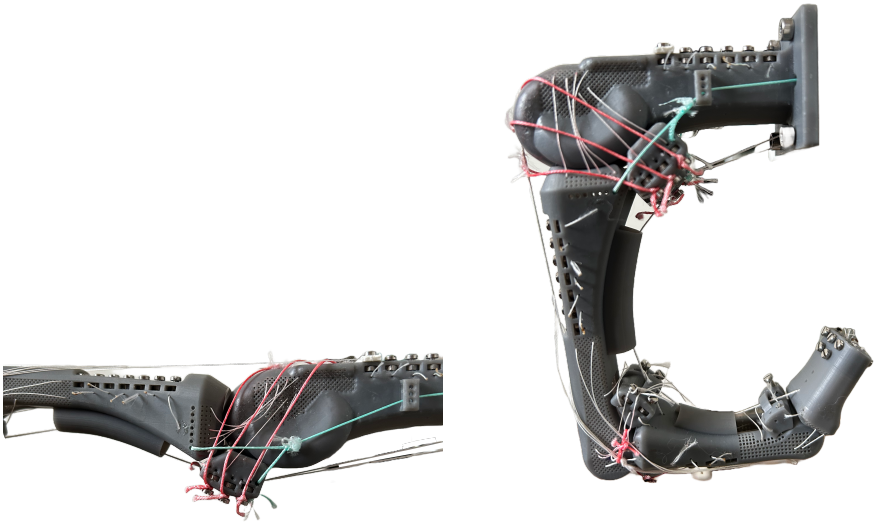

(a) In finger extension, the flexor tendons lie flush against the metacarpal and volar plate.

(b) During MCP joint flexion, the flexor tendons shift toward the pulley, moving away from their position against the volar plate.

Figure A.3: Side view: Flexor tendons change locations at the pulleys, separates from the top surface of the volar plate and metacarpal, increases moment arm

B

Test Setup

The motion capture setup used a six-camera Motive system and a testbed with a force sensor to apply forces to the flexor tendon. Black screens and tape were used to reduce glare and block reflections.

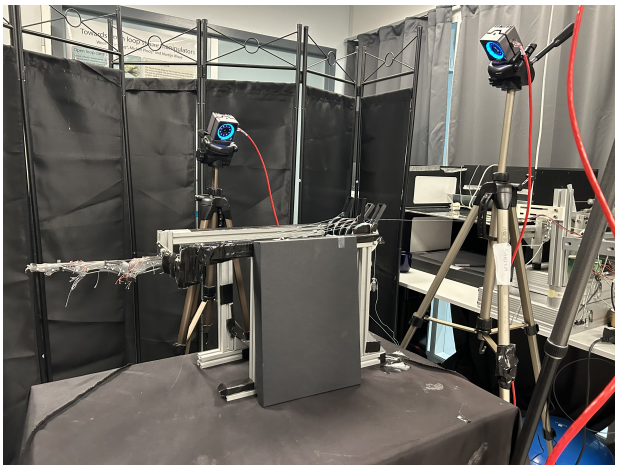

Figure B.1: Test setup, testbed at the end of the pulley system, flexor tendon attached to force sensor

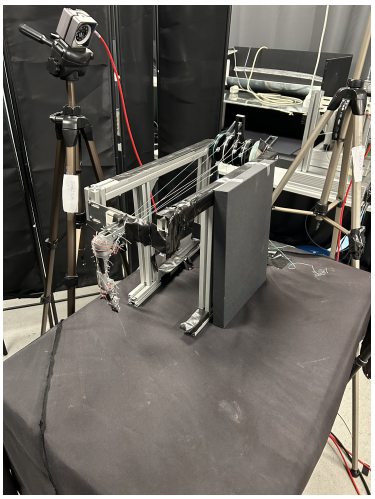

Figure B.2: Top view of the mechanical finger actuation with tendon displacement tracked from small blocks attached to each tendon.

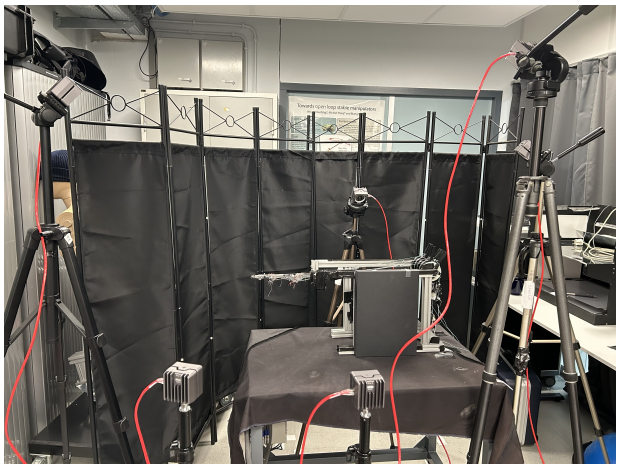

Figure B.3: Six motion capture cameras tracked finger motion and tendon displacement, with three focused on the finger and three on displacement from different heights, angles, and distances.

C

Inverse Kinematics vs Forwards Dynamics Results

Comparison between the joint angles from the IK and FD results for each time step includes: metacarpal joint flexion (MCP flexion), metacarpal joint abduction-adduction (MCP abduction), proximal interphalangeal joint flexion (PIP flexion), and distal interphalangeal joint flexion (DIP flexion). Additionally, the comparison includes experimental force data from the force sensor versus the force calculated from FD results for the flexor digitorum profundus (FDP) tendon, along with the contributions of the forces from the three Lateral Bands, also derived from the FD results.

C.1. Inverse Kinematics (IK)

Inverse Kinematics (IK) results are obtained using the IK Tool, which matches the marker locations from experimental data with those in the OpenSim model to minimize errors. This solver focuses solely on kinematics and does not consider the involvement of muscles in the model.

C.2. Forward Dynamics (FD)

Forward Dynamics is computed by inputting the weight displacement data into the model at each time step, allowing it to calculate joint angles and forces based on the model's states. This simulation incorporates the effects of muscles.

C.3. Results Full Flexion

This experiment begins with the finger in an extended position and involves flexing all the joints by applying a force to the flexor tendon.

C.3.1. Wrapping surface at MCP joint

During the Full Flexion simulations, it was observed that the extensor (ED) tendon and the Lateral Bands slip off the wrapping surface at the MCP joint at approximately 86° in each trial (Figure C.1). This slipping caused a brief (less than 1 second) spike in tendon forces in each trial (Figure C.3). Since this effect is due to a feature in OpenSim and does not significantly impact the overall results or model performance, it was disregarded and excluded from the results.

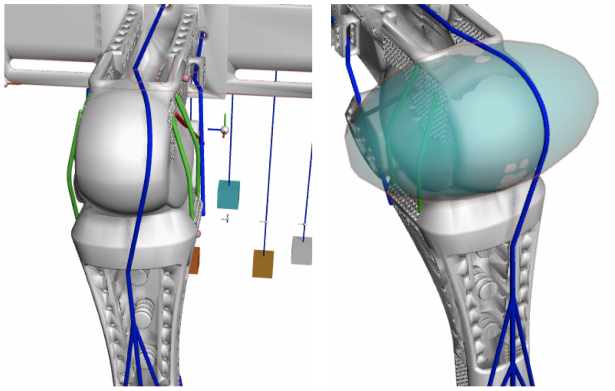

Figure C.1: At each Full Flexion simulation, the ED tendon and lateralbands slip off the wrapping surface (blue, right figure) of MCP joint at an angle of 86 degree (trial 001)

[H]

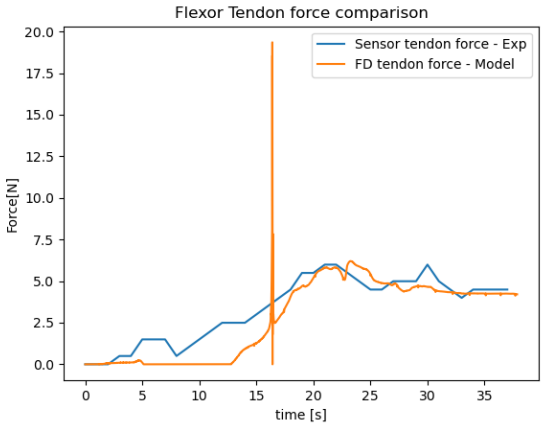

Figure C.2: Flexor tendon force (FDP) between the experimental sensor data and the results from FD Trial 001, observed peak force from ED tendon slipping of the wrapping surface at the MCP joint

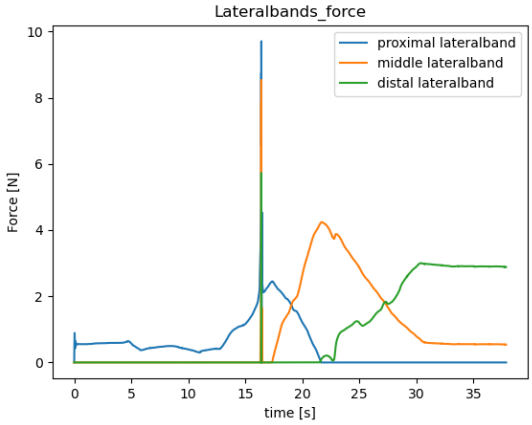

Figure C.3: Forces of the three Lateral Bands from FD Trial 001, observed peak force from ED tendon slipping of the wrapping surface at the MCP joint

C.3.2. Trial 001

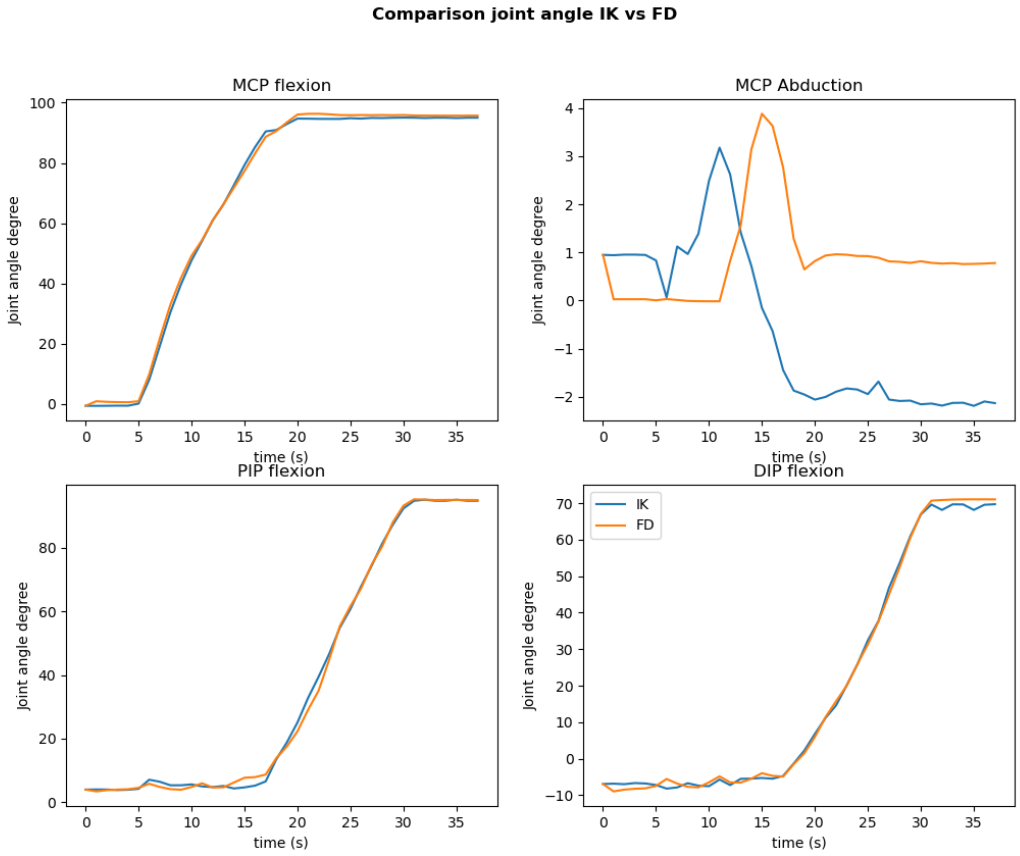

Figure C.4: Full Flexion Trial 001, Joint angles per time step for the IK and FD results

[H]

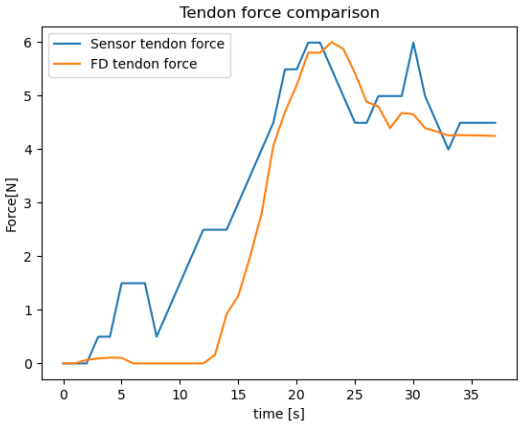

Figure C.5: Flexor tendon force (FDP) between the experimental sensor data and the results from FD Trial 001

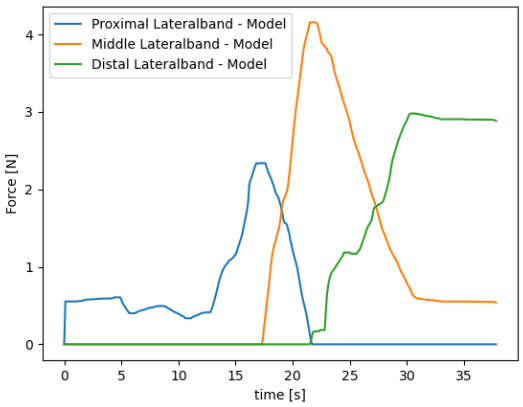

Figure C.6: Forces of the three Lateral Bands from FD Trial 001

C.3.3. Trial 002

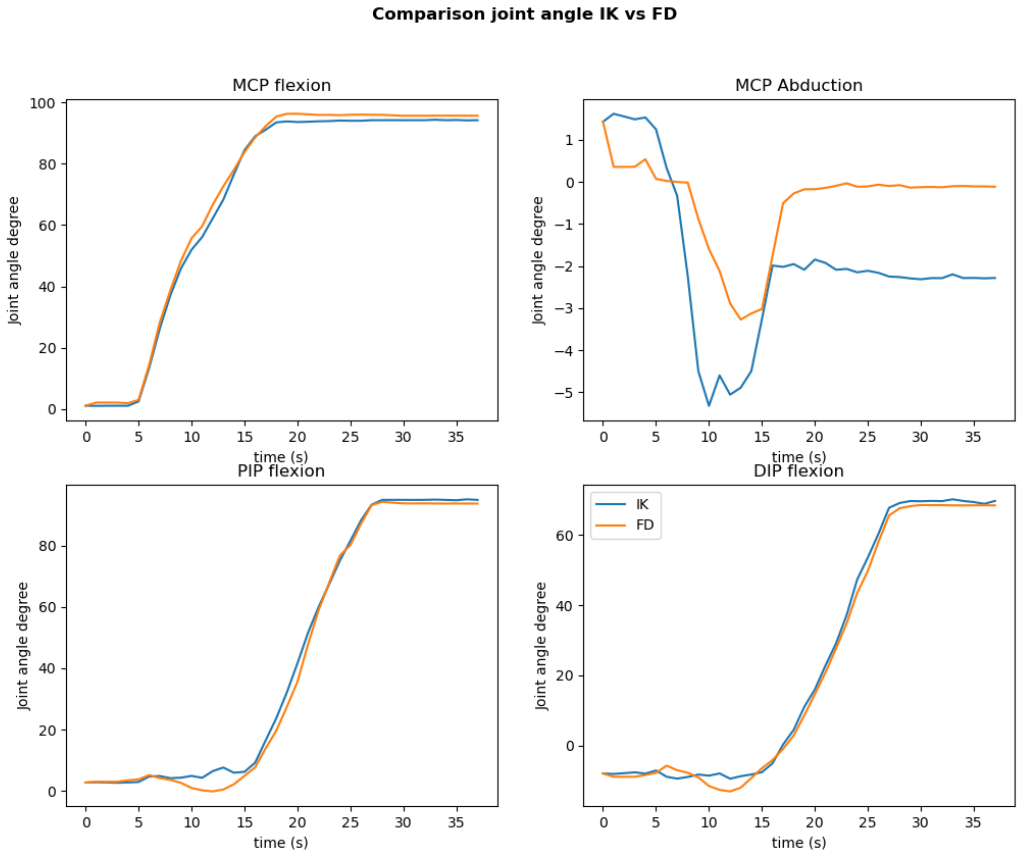

Figure C.7: Full Flexion Trial 002, Joint angles per time step for the IK and FD results

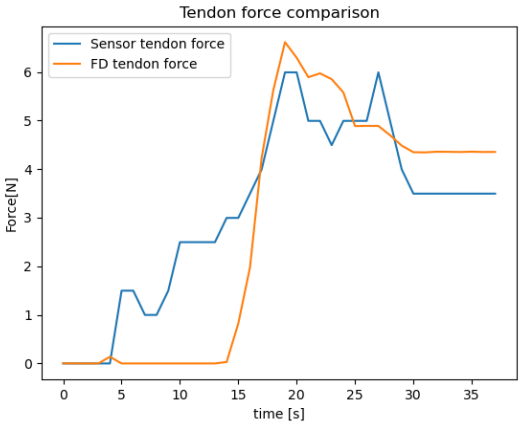

[H]

Figure C.8: Flexor tendon force (FDP) between the experimental sensor data and the results from FD Trial 002

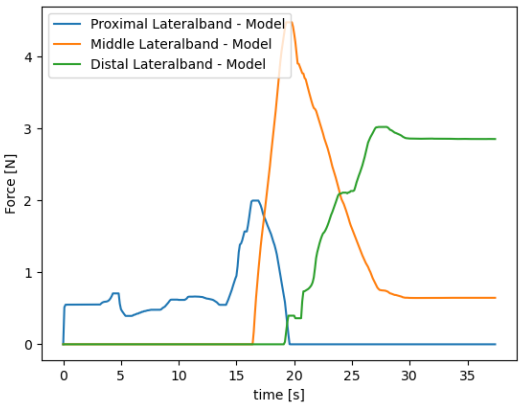

Figure C.9: Forces of the three Lateral Bands from FD Trial 002

C.3.4. Trial 003

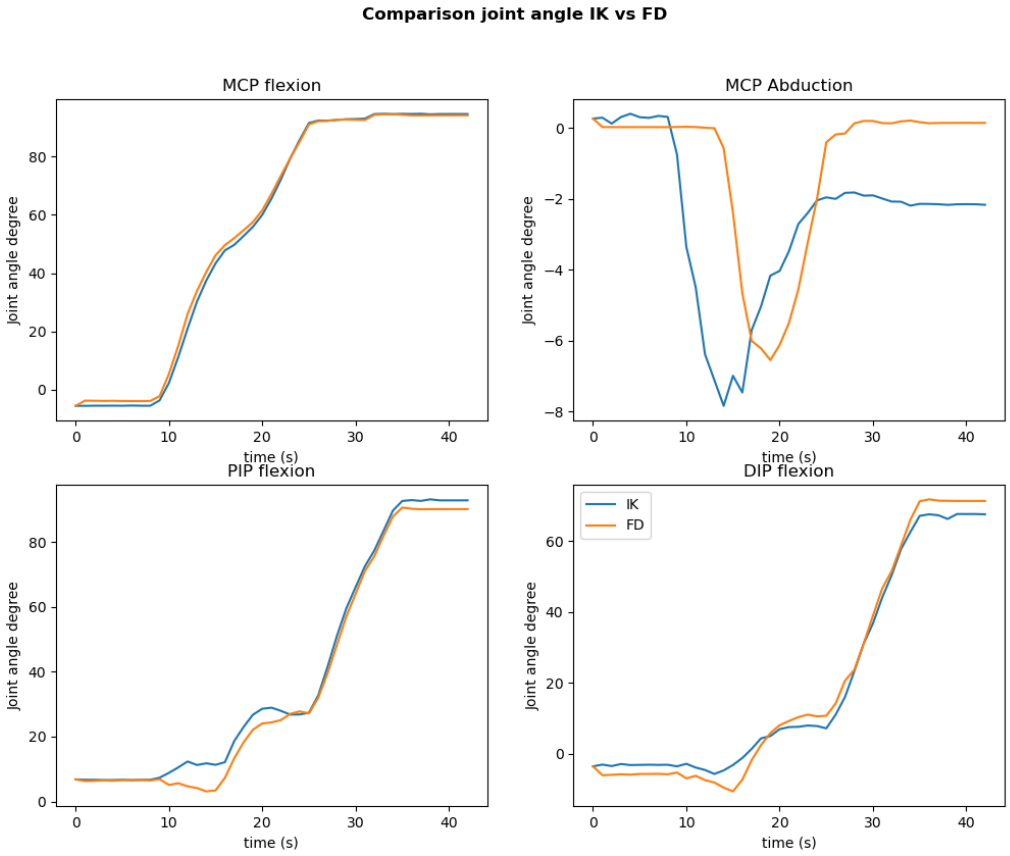

Figure C.10: Full Flexion Trial 003, Joint angles per time step for the IK and FD results

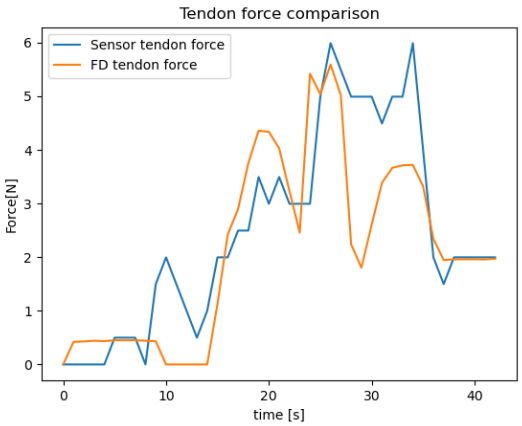

[H]

Figure C.11: Flexor tendon force (FDP) between the experimental sensor data and the results from FD Trial 003

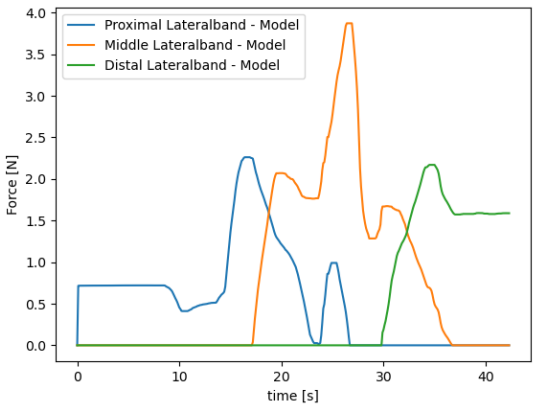

Figure C.12: Forces of the three Lateral Bands from FD Trial 003

C.4. Results IPJ Flexion

This experiment starts from finger extension and flexes only the interphalangeal joints by applying a flexor tendon force and adding a heavy load at the extensor tendon to prevent the MCP joint from flexing as best

as possible.

C.4.1. Trial 001

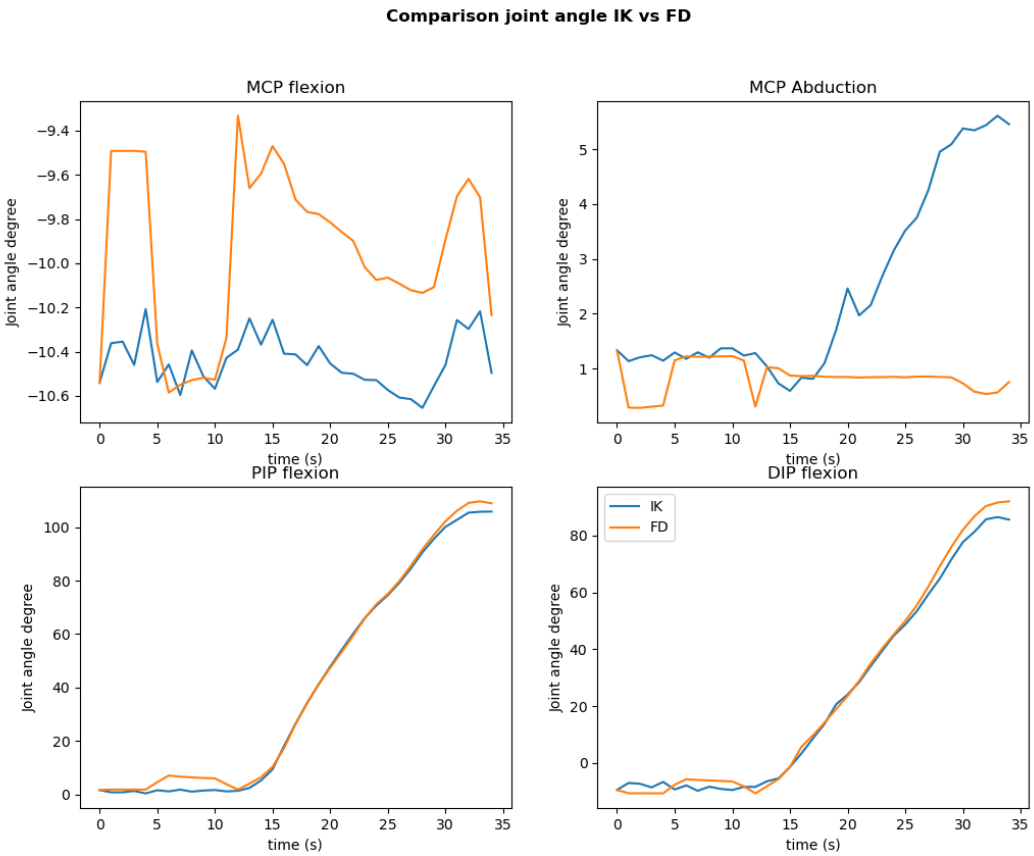

Figure C.13: Full Flexion Trial 001, Joint angles per time step for the IK and FD results

[H]

Figure C.14: Flexor tendon force (FDP) between the experimental sensor data and the results from FD Trial 001

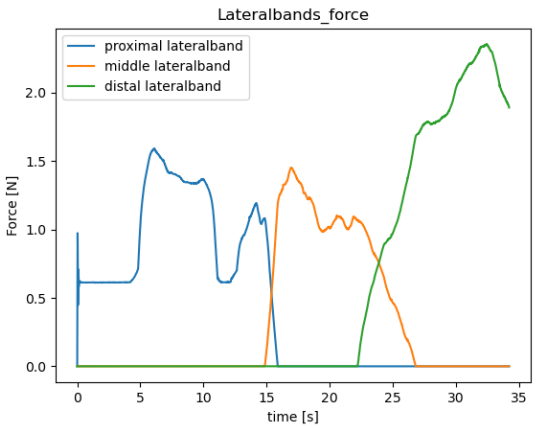

Figure C.15: Forces of the three Lateral Bands from FD Trial 001

C.4.2. Trial 002

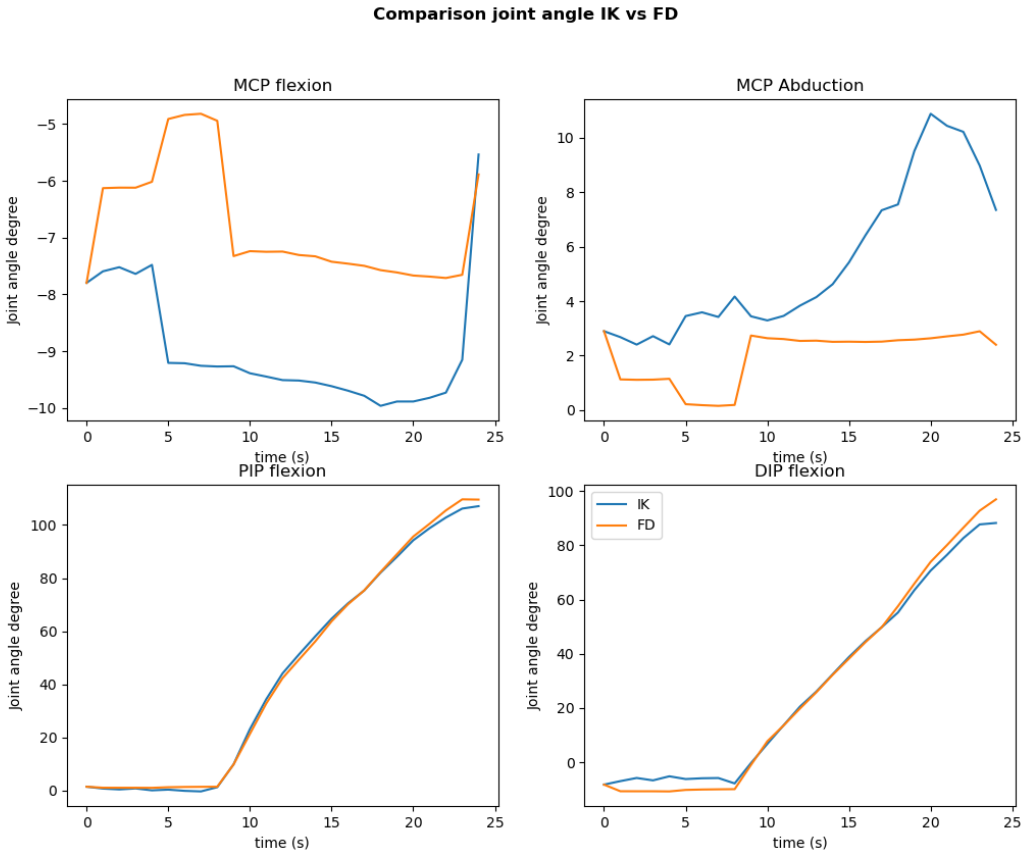

Figure C.16: Full Flexion Trial 002, Joint angles per time step for the IK and FD results

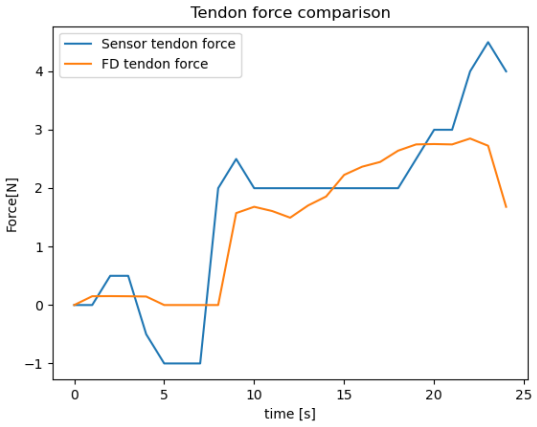

[H]

Figure C.17: Flexor tendon force (FDP) between the experimental sensor data and the results from FD Trial 002

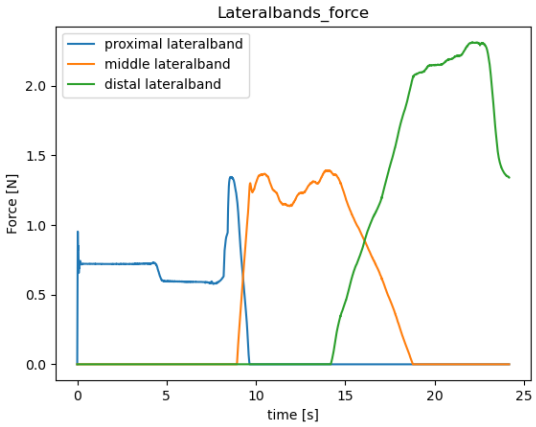

Figure C.18: Forces of the three Lateral Bands from FD Trial 002

C.4.3. Trial 003

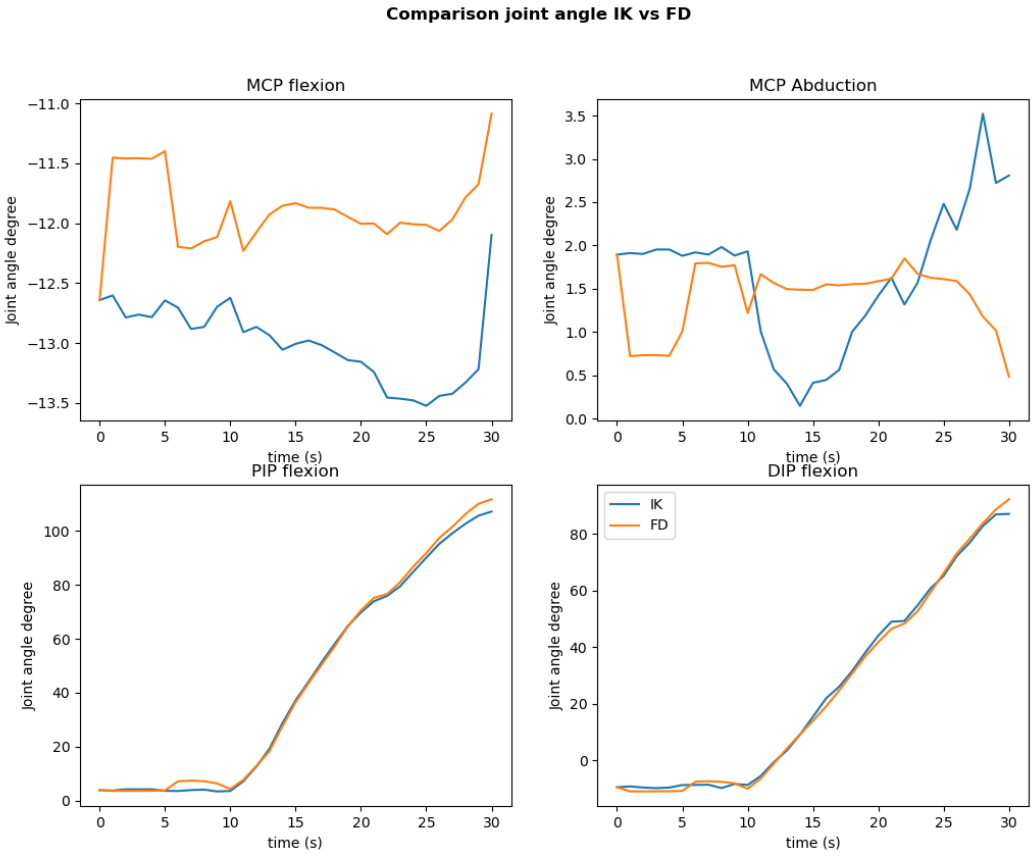

Figure C.19: Full Flexion Trial 003, Joint angles per time step for the IK and FD results

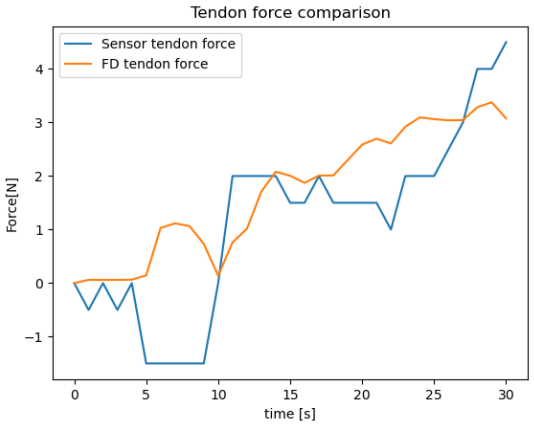

[H]

Figure C.20: Flexor tendon force (FDP) between the experimental sensor data and the results from FD Trial 003

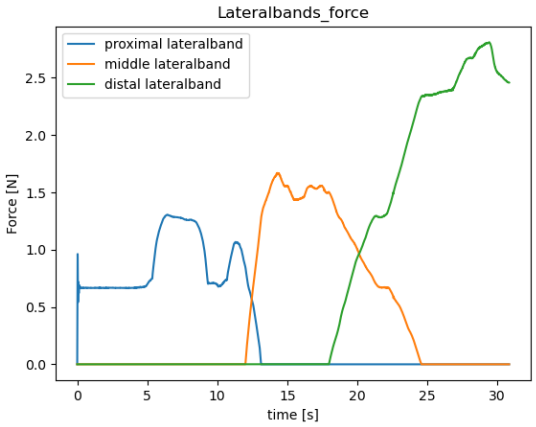

Figure C.21: Forces of the three Lateral Bands from FD Trial 003